Submitted to Physical Review

RECEIVED
LAWRENCE
RADIATION LABORATORY

LBL-256
Preprint c.2

LIBRARY AND
DOCUMENTS SECTION

ANGULAR MOMENTUM OF PRIMARY PRODUCTS FORMED IN THE SPONTANEOUS FISSION OF ^{252}Cf

J. B. Wilhelmy, E. Cheifetz, R. C. Jared
S. G. Thompson, H. R. Bowman, and J. O. Rasmussen

October 1971

AEC Contract No. W-7405-eng-48

TWO-WEEK LOAN COPY

This is a Library Circulating Copy which may be borrowed for two weeks. For a personal retention copy, call Tech. Info. Division, Ext. 5545

LAWRENCE BERKELEY LABORATORY
UNIVERSITY OF CALIFORNIA
BERKELEY

LBL-256
c.2

34

DISCLAIMER

This document was prepared as an account of work sponsored by the United States Government. While this document is believed to contain correct information, neither the United States Government nor any agency thereof, nor the Regents of the University of California, nor any of their employees, makes any warranty, express or implied, or assumes any legal responsibility for the accuracy, completeness, or usefulness of any information, apparatus, product, or process disclosed, or represents that its use would not infringe privately owned rights. Reference herein to any specific commercial product, process, or service by its trade name, trademark, manufacturer, or otherwise, does not necessarily constitute or imply its endorsement, recommendation, or favoring by the United States Government or any agency thereof, or the Regents of the University of California. The views and opinions of authors expressed herein do not necessarily state or reflect those of the United States Government or any agency thereof or the Regents of the University of California.

ANGULAR MOMENTUM OF PRIMARY PRODUCTS FORMED IN THE SPONTANEOUS FISSION OF ^{252}Cf*

J. B. Wilhelmy, E. Cheifetz,† R. C. Jared,
S. G. Thompson, and H. R. Bowman

Lawrence Berkeley Laboratory
University of California
Berkeley, California 94720

and
J. O. Rasmussen

Chemistry Department
Yale University
New Haven, Connecticut 06520

October 1971

ABSTRACT

The measured intensities of intra-band cascading transitions in the ground state bands of 21 high yield even-even fission products have been analyzed by two methods to determine the magnitude of the intrinsic angular momentum of the primary products formed in the spontaneous fission of ^{252}Cf. The first method was to quantitatively compare the intensities of the intra-band transitions observed in fission with those reported in the literature for in-beam (particle, xn) reactions for which the primary angular momentum distribution was determined by optical model calculations. The second method was based on a simple statistical model analysis of the angular momentum distribution throughout the neutron evaporation and the pre-ground state band gamma ray transition phases of the de-excitation process. The two methods gave reasonably similar results with the former method yielding a somewhat larger primary

angular momentum for the fragments. The general conclusions from the statistical model analysis are that: (1) the average angular momentum of the products is $\bar{\ell} \approx 7 \pm 2\ \hbar$, (2) the heavy fission products have $\approx 20\%$ greater angular momentum than the light products, (3) the more symmetric the mass division the lower the initial angular momentum and, (4) there are only small changes in angular momentum ($\sim 1\text{-}2\hbar$) with changes in fragment kinetic energy. An important feature of these results is that the fragment angular momentum does not correlate with the number of neutrons evaporated by the fragment. Additional measurements have been made to study the angular distribution of individual prompt gamma rays. In all observed cases the $2^+ \rightarrow 0^+$ ground state transitions were forward peaked with respect to the fission axis, and this is consistent with the assumption that the angular momentum is aligned in a plane perpendicular to the direction of fission. The results are discussed in terms of a quasi-statistical model in which the neck width at scission is approximately constant.

I. Introduction

The angular momentum distribution in the primary fission fragments has been of experimental and theoretical interest as it provides information on the properties of the fissioning nucleus from the time it goes through the saddle point until shortly after scission. The angular momentum distribution of the fragments in particular bears a close relationship to vibrations of matter in the neck normal to the fission direction.[1] At scission this results in angular momentum of the fragments normal to their axis of separation; thus angular momentum is induced even in fragments from spontaneously fissioning nuclei such as ^{252}Cf which originally have spin zero. A different picture of the fissioning nucleus is one in which the fragments at scission have their tips directed along a line of centers. A finite distribution of rotational angular momentum is introduced through the uncertainty principal relationship between angular position and momentum.[2] Coulomb excitation between the separating fragments can also alter the angular momentum distribution present at scission. Since the characteristics of the gamma-ray de-excitation of the fragments are particularly sensitive to the magnitude and orientation of the angular momentum of the fragments, studies of gamma-ray emission from fission have provided most of the knowledge about the angular momentum in fission. Previous estimates of angular momentum have been based on three kinds of information concerning the γ-ray de-excitation:

(a) Angular distribution of the gross unresolved prompt γ-rays. These studies were performed using neutron induced fission of ^{233}U, ^{235}U, and ^{239}Pu and spontaneous fission of ^{252}Cf by several groups.[3-7] In all the experiments anisotropy with preferential emission of 10-15% more γ-rays in the fission direction relative to the direction normal to the fragments was found. Valskii[8,9] and Armbruster[10] have further investigated this anisotropy as a function of mass ratio and total kinetic energy of the fission events and have found the anisotropy to be rather independent of these quantities. The interpretation of these experiments in terms of J is based on Strutinskii's derivation[11] of the angular distribution of the broad γ-rays which to first order is

$$W_L(\theta) = 1+k_L(\hbar^2 J/\mathcal{J}T)^2 \sin^2\theta$$

where θ is the angle of emission of the γ-ray with respect to the fragment direction; $k_L = +1/8$, $-3/8$ and $-81/64$ for $L = 1,2,3$ respectively where L is the multipolarity of the radiation. $\mathcal{J}$ is the moment of inertia and T is the nuclear temperature. The derivation of J depends thus on assuming the radiation to be predominantly E2 in character and it also depends in a very sensitive way on assumptions regarding the values of T and $\mathcal{J}$ which are quantities not determined experimentally. The proposed values of J based on the same experimental results varied between $(\bar{J}^2)^{1/2} = 4.4$ to 20 depending on model assumptions.

(b) Studies of γ-ray multiplicities and total energy in fission. It was found that the total γ-ray energy in the thermal neutron induced fission of ^{235}U was ~7.2 MeV[12] and this is larger than that which would be expected from the average neutron binding energies if no angular momentum

were present. Thomas and Grover[13] have calculated the γ-ray energy and multiplicity using appropriate spin dependent level density expressions. They found that the experimental results are consistent with assuming $\bar{J} = 5.5$.

(c) Isomer yield experiments. The ratios of independent yields of isomers relative to independent ground state yields have been studied for several suitable fission products such as: ^{81}Se and ^{83}Se,[14] ^{134}Cs,[15] ^{131}Te and ^{133}Te.[16] The experimental ratios have been interpreted using the method of Huizenga and Vandenbosch.[17] This method employs a statistical treatment of isomer ratios with spin cut-off parameters that are fitted to data for which the input angular momentum is known. From this analysis the value of $\bar{J}$ determined in thermal neutron fission of ^{235}U and other induced fission cases was in the range of about 5.5 to 8$\hbar$.

The new approach which we present in this paper for the determination of angular momentum is based on the results of recent experiments in which the energies and intensities of prompt transitions de-exciting the 2^+, 4^+, 6^+ and 8^+ levels of the ground state bands in many even-even fission products have been measured.[18-20] Two different methods were then employed to estimate the initial angular momenta of the fragments. The first method involved comparison of the relative intensities obtained from our experimental data with the corresponding relative intensities from the decay of nuclei produced in reactions for which the initial angular momentum distribution could be calculated. The second method involved statistical analysis similar to that used by Huizenga and Vandenbosch[17] to interpret the isomer ratio data. The results are quite similar to those from analysis of isomer ratio data. However, since data from 37 even-even fission isotopes have been obtained

from our experiments, a correlation can be obtained for a wide variety of specific products covering the region of fission fragments with high yields.

An additional experiment to measure the angular distributions of gamma rays of several of the known $2^+ \rightarrow 0^+$ transitions showed that they are emitted preferentially in the fragment direction. This provides direct evidence that the primary angular momentum is aligned normal to the fission direction. The magnitude of the anisotropy is consistent with the magnitude of J obtained by the statistical analysis method.

II. Experimental

Information about the intrinsic angular momentum of the primary fission products was obtained from two separate experiments. In the first experiment the intensities of ground state band transitions in even-even fission products were measured. The experiment consisted of three or four parameter coincidence measurements where the kinetic energies of the two fission products formed in the spontaneous fission of ^{252}Cf were measured simultaneously with: a) single gamma rays, b) two gamma rays, and c) gamma rays and K x-rays. The details of these experiments have been presented elsewhere[18-20] and only a brief description will be given here. Figure 1 shows a schematic representation of the experimental configuration for the four parameter measurements. A source of $\sim 10^5$ fissions/min was electrodeposited on the surface of detector F_1. In this procedure fragments entering the detector were stopped in $\sim 10^{-12}$ sec and, therefore, transitions having life times longer than this value were not Doppler shifted and were sharp when recorded in the photon detectors.

The masses of the fission fragments were determined from the measured kinetic energies. The measurements of the prompt gamma rays in coincidence with a specific K x-ray were used to assign the transitions to specific elements. Once transitions were assigned to specific isotopes gamma-gamma coincidence measurements were performed to establish cascade sequences in the de-excitation process. Quantitative information regarding intensities were determined using the higher efficiency inherent in a three parameter experiment in which the two fragment kinetic energies were measured in coincidence with prompt gamma rays. With this technique the intensities of transitions de-exciting ground state bands of 37 even-even fission product nuclei have been determined.

Details about the identification of the ground state band transitions in even-even fission fragments were reported in Ref. 18 for light fragment and Ref. 19 for heavy fragments. The summary of the intensities of the ground state band transitions from nuclei produced by the spontaneous fission of ^{252}Cf was presented in Table 1 of Ref. 21. The intensities presented there have been corrected for internal conversion and for any delayed transitions in the de-excitation process. Systematic errors are perhaps present in the case of any transitions with half lives shorter than 10^{-12} sec. Since such gamma rays could still be emitted by the moving fragment before it stopped in the plated detector. Thus these gamma rays would appear partially Doppler shifted and broadened. Since only sharp unshifted transitions were studied an underestimate of the total transition intensity was possible. This remark applies specifically to the intensities of the $2^+ \rightarrow 0^+$ transitions in ^{98}Zr (1223 keV), ^{134}Te (1278 keV) and ^{136}Xe (1313 keV).

The second experiment was an angular distribution study in which the intensities of individual γ-rays were measured relative to the fission fragment axis. The experimental configuration is schematically presented in Fig. 2. A source with a diameter of about 2mm and approximately 10^6 fissions/min of ^{252}Cf was electrodeposited onto a 0.005 inch thick platinum foil. Prompt fission gamma rays were recorded in coincidence with fission fragment kinetic energies. A 1 cm^3 Ge(Li) detector having resolution of 1.2 keV at 280 keV was used for the gamma ray measurements. The fission fragment kinetic energies were recorded in any of three phosphorous diffused 300 ohm-cm fission fragment detectors which were located approximately 3.5 cm from the source foil. Each detector had an area of 300 mm^2. The fragment detectors were used for timing purposes to insure that only prompt fission gamma rays were recorded and also to establish the fission axis about which the gamma ray distributions were observed. By using three fission fragment detectors the intensities of transitions were determined at three different angles in one experimental run. Since the kinetic energy of only one fragment from each pair was measured (the other fragment was always stopped in the Pt backing) the gamma rays were sorted only according to whether they were associated with light or heavy fragments. Two experimental runs, each of about one week duration, were performed in order to obtain information on transition intensities at six different angles (90°, 67.5^o, 45°, 22.5^o, 0° and -22.5^o) one of which (-22.5^o) was chosen to be redundant for consistency determinations. The data were stored in an on line PDP-9 computer. The intensities of gamma transitions were obtained using a computer code for gamma ray analysis developed by Routti and Prussin.[22] Three γ-ray spectra

associated with light fragments stopped in the Pt backing and obtained at angles 0°, 45°, and 90° to the fragment are shown in Fig. 3.

It was not possible to determine experimental angular distributions for all transitions observed in the experiment. There were two reasons for this limitation. The first was that the very complex gamma-ray spectra could not be sorted according to mass; and therefore only intensities of strong transitions which were ascertained in the mass sorted data of the three and four parameter experiments to be relatively free of interfering radiations could be accurately determined. The second difficulty was that the gamma rays emitted in flight by the complementary fragment were Doppler shifted due to the high fragment velocity. The energy shift observed in the laboratory frame was dependent on the angle of observation. Therefore many gamma rays emitted from fragments stopped in the Pt backing had interfering radiations shifted into their peak positions at certain observation angles thus obscuring intensity determinations. Even with these limitations it was possible to obtain angular distribution data for 12 discrete transitions where interferences were small. Of these transitions seven were associated with the ground state bands of even-even fission products and all of these showed forward peaking. The measured intensities of the fitted gamma rays are presented in Table 1 as a function of angle relative to the fission axis. The uncertainty of the relative intensities was assumed to be 10%. This value exceeds the statistical uncertainty of the fits but was deemed necessary due to the arbitrary requirements of linear background imposed by the fitting routine. The angular distribution coefficients were extracted by making least

squares fits to the measured gamma ray intensities as a function of angle with respect to the fission axis. The expression used was:

$$W(\theta) = A_o \left[1 + a_2 P_2(\cos\theta) + a_4 P_4(\cos\theta) \right] . \qquad (1)$$

Since some of the fits to the data do not lead to a significant value of a_4 the fits were also made with $a_4 = 0$.

The a_2 and a_4 coefficients were corrected for the finite solid angle subtended by the detectors. The solid angle correction factor for a_2 was 0.917 and for $a_4 = 0.744$. The corrected values of a_2 and a_4 are shown in Table 1.

The anisotropy in the angular distribution of some of the transitions could possibly be influenced by attenuation due to extra-nuclear effects. All the $2^+ \rightarrow 0^+$ transitions that were observed have half life values of 0.2 - 2 nsec. (The life time was found in previous experiments from Doppler shift considerations). The attenuation in the angular distributions inside the Pt host is dependent on the electronic structure and is, for any element, largest for transitions with longer half life values as can be seen for the cases of the two isotopes ^{104}Mo and ^{106}Mo. The results of anisotropies can thus be looked upon as lower limits of the real values with a_2 values of shorter lived $2^+ \rightarrow 0^+$ transitions such as ^{110}Ru being close to the actual values. Angular distribution results are shown in Fig. 4 for some transitions. The results clearly show that there is alignment of the angular momentum in the fission process. The two transitions shown associated with the even-even isotopes are the $2^+ \rightarrow 0^+$ ground state transitions and therefore are lowest members of a cascade of stretched E2 transitions. The observed intensities for these stretched E2 transitions are forward peaked implying that the angular momentum is

initially aligned in a plane perpendicular to the fission axis. The 95 keV transition associated with the odd A isotope ^{105}Mo is seen to have an anisotropy peaked at 90°. This is consistent with its being a stretched predominately M1 transition that is possibly a member of a cascading band.

III. Analysis

A schematic representation of the de-excitation process of the primary fission fragments is shown in Fig. 5. The fragments after scission can be visualized as tumbling about the axis of separation with their angular momentum aligned in a plane perpendicular to this axis. In addition to the high kinetic energy of the initial fragments they also possess substantial internal excitation energy which is dissipated through evaporation of neutrons and emission of gamma rays. Since only the last stages of the de-excitation process are observed in these experiments the quantitative determination of the angular momentum after scission requires consideration of the changes in angular momentum induced in the evaporation and statistical gamma emission processes. As mentioned previously this analysis was performed utilizing two methods.

A. Reaction Comparison

The first method of analysis which was used to interpret the experimental data simply consisted of a comparison of the intensities of the prompt-fission gamma rays with those observed in in-beam gamma-ray studies of (charged particle, xn) reactions. In recent years in-beam gamma-ray spectroscopy has become a fruitful area of research and appreciable amounts of nuclear structure information are being currently

obtained. The significant features of these reactions are: (1) A substantial amount of angular momentum is introduced in the compound nucleus through the reaction collision; (2) the angular momentum is aligned in a plane perpendicular to the beam axis; (3) the majority of the excitation energy is removed by neutron evaporation; (4) the angular momentum is dissipated through cascading band transition as the residual nucleus de-excites toward its ground state. This situation is therefore quite analogous to the de-excitation of the prompt fission products. By comparing the intensities of transitions de-exciting the ground state bands of even-even fission products with those observed in reactions of the type A(charge particle, xn)B for which the initial angular momentum could be calculated and B is even-even, it is possible to obtain information on the primary angular momentum of the fission products.

This method of estimating the angular momentum of the fragments is direct and requires no model assumptions regarding the de-excitation process. The only assumption implicit in this method is that the induced distribution of angular momentum in the reactions is not radically different from the fission product primary angular momentum distribution. The former distributions tend to be of the form $(2L+1)T_L$, with T_L the optical model transmission coefficient, usually resembling a Fermi function of unity for low L values and zero for high L values. The latter distribution has been suggested by Nix and Swiatecki[1] to have the shape of $(2L+1) \exp(-L^2/B^2)$ in which B is a parameter related to the nuclear stiffnesses about normal modes. Despite the differences in distribution functions we assume that average L values in fission can be deduced by these comparisons to an accuracy consistent with other uncertainties from the statistical de-excitation paths.

Figure 6 presents the experimental data on the observed intensities of transitions de-exciting ground state bands in even-even nuclei. All transition intensities are normalized so that the $2^+ \rightarrow 0^+$ transition intensities in each nucleus are assigned the value of one. The lines join the reported experimental intensities of transitions associated with specific reactions. The lines are labeled with the average angular momentum induced in the compound nucleus. These values have been calculated using optical model codes.[23] The reactions and bombarding energies used for Fig. 6 are presented in Table 2. The most important feature of the reaction data presented in Fig. 6 is that there appears to be a good positive correlation between the intensities of transitions observed in the ground state bands with the average angular momentum present in the compound nucleus. It should be pointed out that this correlation persists even though a wide range of projectiles and bombarding energies were used [(p,2n) at 12 MeV to (^{14}N,5n) at 93 MeV]. Furthermore there were a variety of residual nuclei produced ranging from isotopes considered nominally spherical (^{118}Te) to deformed isotopes in the center of the rare earth region. This correlation is not perfect. It is seen that the line labeled $\bar{\ell}$ = 11.0 crosses two other lines which implies that some transitions in the ground state band appear to have an intensity which is slightly too large. Also the line labeled $\bar{\ell}$ = 22 is seen to have a local maximum intensity at ℓ = 8 which is inconsistent with the assumptions that once the nucleus is in the ground state band it can only cascade through the lower spin members. The implication of the local maximum is that part of the population of the 8^+ level does not cascade to the 6^+ member of the ground

state band. It should be emphasized that these apparent anomalies could well be attributed to experimental uncertainties. No attempt was made to adjust or make value judgments on the reported literature results. Also shown in Fig. 6 are relative intensities of the complementary fission product nuclei ^{104}Mo and ^{144}Ba. These data points are seen to be between the lines labeled $\bar{\ell} = 8.0$ and $\bar{\ell} = 9.6$. A linear interpolation of the experimental intensities for ^{144}Ba gives an $\bar{\ell}$ value of 9.2.

B. Statistical Model Analysis

The second method consisted of a simple statistical model analysis which was based on methods developed by Huizenga and Vandenbosch[17] to explain isomeric yield ratios in neutron capture and charged particle reactions. This model assumes that the distribution of levels with specific spin is given by:

$$P(J) \propto (2J+1) \exp\left[(-J+1/2)^2/2\sigma^2\right] \qquad (2)$$

Where P(J) is the probability distribution of levels with spin J and σ is a parameter which limits the population of high spin levels and is in principle related to the moment of inertia and the temperature of the excited nucleus. The de-excitation from a specific spin level by a transition is assumed to populate residual spin levels with a probability dependent on the availability of the specific levels as given in equation 2. A further assumption is that following neutron capture or after completion of the neutron evaporation the residual nucleus emits three E1 gamma rays before reaching the isomeric level or ground state. With these assumptions a large variety of isomeric yield data were empirically correlated using for σ a value of three or four. Once the value of σ was experimentally established for cases in which the initial angular momentum was either

known or could be calculated this technique was applied, using the predetermined value of σ, to extract information on the magnitude of the angular momentum in fission. This method was applied to fission products by Warhenek and Vandenbosch[15] to interpret the primary angular momentum of fission products. They experimentally determined the prompt independent yields of the isomeric level and ground state in ^{134}Cs for the reactions: $^{233}U(\alpha_{42},f)$, $^{233}U(\gamma_{16},f)$, $^{235}U(\alpha_{27},f)$, $^{238}U(\alpha_{30,42},f)$ and $^{237}Np(d_{21},f)$. They assumed the probability distribution of initial angular momentum states of the fragments could be represented by:

$$P(J) \propto (2J + 1) \exp [-J(J+1)/B^2] \qquad (3)$$

Where P(J) is the probability distribution for each spin value J and B is approximately equal to the rms value of $(J + 1/2)$. This functional form which was originally chosen from statistical considerations has, however, also been predicted on theoretical grounds by Nix and Swiatecki[1] and by Rasmussen et al.[2]

This statistical analysis was also applied to fission fragment angular momentum determinations by Sarantities, Gordon and Coryell.[16] They experimentally determined the independent yields of the isomeric levels and ground states in ^{131}Te and ^{133}Te for the following induced fission reaction: $^{235}U(n_{th},f)$, $^{232}Th(\alpha_{33},f)$, $^{232}Th(d_{18},f)$, $^{238}U(\alpha_{33},f)$, $^{238}U(d_{18},f)$. Using the same functional form for the primary angular momentum as Warhanek and Vandenbosch, they extracted a value of $B = 6 \pm 1.5$ for the $^{235}Th(n_{th},f)^{131}Te$ reaction. This value corresponds to an average primary angular momentum of $5.0 \pm 1.5\ \hbar$ for fission events leading to the formation of the Te isotopes. They found, similar to the results of Warhanek and Vandenbosch,

that there was an apparent slight increase in the fragment angular momentum with increasing excitation energy and angular momentum of the compound nucleus. For the reaction $^{232}Th(\alpha_{33},f)^{131}Te$ they found the average angular momentum of the primary fragment to have increased to ~7 from the value of 5 ± 1.5 for the reaction $^{235}U(n_{th},f)$.

We have also applied this statistical analysis to interpret the primary fragment angular momentum using instead of the population of isomeric levels, the experimentally determined intensities of transitions de-exciting the ground state bands in even-even fission product nuclei. By using the prompt gamma ray data we have four principal advantages when compared with the previous methods:
(1) it is not necessary to have a fission product which has a convenient isomer, (2) it is possible to obtain information on the highest yield prompt products, (3) for each product we have population information for up to four spin levels (the 2^+, 4^+, 6^+, 8^+ from the gamma ray intensities) instead of just two points as in the isomer studies, (4) it is in principle possible by using the presented technique to correlate the angular momentum with other fission variables such as kinetic energy. We have evaluated the intensities of the members of the ground-state bands of even-even fission products and using equation 3 have extracted the value of B, the only free parameter in the model. Explicitly, the calculational procedure consisted of: (1) determining the average number of neutrons emitted from each residual nucleus by correcting the average neutron emission results of Bowman et al.[29] using current results on post neutron emission mass determinations for the even-even fission products; (2) evaluating

the angular momentum removed by each neutron by determining the partial wave amplitudes using transmission coefficients derived from a simple square well potential;[30] (3) for neutron evaporation a value of $\sigma = 4$ was used in equation 2 to determine the availability of specific levels; (4) as a function of the parameter B(equation 3), coupling the probability of emission of various partial wave neutrons in proportion to the availability of the allowed spin levels (Fig. 7 presents a schematic example for the spin distribution in the residual nuclei for various steps in the neutron evaporation); (5) after neutron emission it is assumed that there are three dipole transitions statistically emitted before reaching the ground state band (the results are not changed significantly if E2 transitions are assumed); (6) the change in angular momentum from the emission of each of these gamma rays is determined by coupling the $\ell = 1$ multipolarity for each transition in proportion to the availability of allowed spin levels as given by equation 2 using a value of $\sigma = 3$; (7) after the statistical emission of gamma rays it is assumed the ground state band is fed directly and the intensities of the cascading intra-band transition are evaluated.

An example of the results of this analysis are shown in Fig. 8 for the residual isotope ^{144}Ba as a function of the parameter B. The experimental data are within a band defined by B = 6 and B = 8, and a simple linear interpolation gives a value of $\overline{B} = 7.2$ for this isotope. Using this analysis procedure similar information was extracted for 21 isotopes. The results of the analysis are presented in Table 3.

A further application of the statistical model is a prediction of the degree of nuclear spin alignment at each stage of the de-excitation process. As pointed out by Hoffman[4] and Nix and Swiatecki[1] the angular momentum of the primary fragments would be expected to be initially aligned in a plane perpendicular to the fission axis. This initial alignment will be partially destroyed through the neutron evaporation and gamma ray transitions steps. If we make the assumption that the reduced nuclear transition matrix elements between various states are constant, the quantitative determination of the disalignment reduces to a geometry problem which can be evaluated by summing over Clebsch-Gordon coefficients weighted by the probability distribution of the available states. This distribution can be represented as:

$$P(J'M') = \sum_{J_I=J_{min}}^{J_I = J_{max}} \cdot \sum_{M_I=J_I}^{J_I} P(J_I M_I) \cdot \sum_{\ell=0}^{\ell=\ell_{max}} T(\ell) \cdot$$

$$\sum_{J'=|J_I-\ell|}^{J_I+\ell} \frac{\exp[-(J'+1/2)^2/2\sigma^2]}{\left\{\sum_{J'=|J_I-\ell|}^{J_I+\ell} \exp[-(J'+1/2)^2/2\sigma^2]\right\}} \cdot$$

$$\sum_{M_e=-\ell}^{\ell} (J_I, M_I, \ell, M_\ell \mid J', M_I+M_\ell)^2 \qquad (4)$$

$$P(J_f M_f) = \sum_{J'=J'_{min}}^{J'=J'_{max}} \cdot \sum_{M'=-J'}^{J'} P(J'M') \cdot \sum_{J_f=|J'-1/2|}^{J'+1/2} \frac{\exp[-(J_f+1/2)^2/2\sigma^2]}{\left\{\sum_{J_f=|J'-1/2|}^{J'+1/2} \exp[-(J_f+1/2)^2/2\sigma^2]\right\}} \cdot$$

$$\sum_{M_s=-1/2}^{1/2} (J',M',\ 1/2,M_s|J_f,M_f)^2 \qquad (5)$$

where the P(J,M) terms are the relative population of the specific states (J,M) at the initial, intermediate and final values for the transitions; $T(\ell)$'s are the transmission coefficients for the neutron evaporation;[30] and σ is the spin cut off parameter which was assumed equal to 4 for neutron evaporation and equal to 3 for gamma emission. After scission the initial spin distribution is given by Eq. 3 with the assumption that all $M \neq 0$ states are zero. The above expressions were summed for each evaporated neutron. For the statistical gamma emission Equation 4 was used with the sum over ℓ and the $T(\ell)$ terms eliminated since only dipole radiations were considered.

With the angular distribution expression

$$W(\theta) = 1 + a_2P_2(\cos\theta) + a_4P_4(\cos\theta)$$

it is possible to calculate the angular correlation coefficients a_2 and a_4 for cascading quadrupole transitions within the ground state band if the relative population of the M substates are known. Rasmussen and Sugihara[31] give the general formula for the angular correlation coefficients:

$$a_k(J) = \frac{a_k^o(J)}{P_k(0)} \sum_{M=-J}^{J} W(M)P_k(M/[J(J+1)]^{1/2}). \qquad (6)$$

where k is the order of the coefficient, P_k is the Legendre polynomials, W(M) is the normalized distribution of magnetic substates with spin J, and a_k^o (J) is the angular correlation coefficient for stretched quadrupole transitions from levels of spin J which are perfectly aligned.[31]

It should be emphasized that these alignment calculations involve no additional assumptions and include no new free parameters. They therefore can be regarded as a further test for any statistical model analysis. The experimental angular distribution of the $2^+ \rightarrow 0^+$ transitions provides direct evidence that the fragments' primary angular momenta are aligned predominantly normal to the axis of separation of the fission fragments. Defining the axis of quantization along the fission direction the population of the various m - magnetic substates of the 2^+ state can be calculated exactly from the observed angular distribution of the $2^+ \rightarrow 0^+$ transition which has the form $W(\theta) = 1+a_2P_2(\cos\theta) + a_4P_4(\cos\theta)$.

Following de Groot et al.[32] the population of the various m components α_m can be represented as:

$$\alpha_0 = 0.20 + 0.40\ a_2 - 0.30\ a_4;$$

$$\alpha_{\pm 1} = 0.20 + 0.20\ a_2 + 0.20\ a_4;$$

$$\alpha_{\pm 2} = 0.20 - 0.40\ a_2 - 0.05\ a_4.$$

The populations of the various m substates of the 2^+ level of ^{144}Ba are shown in Fig. 9, clearly demonstrating that the angular momentum of that state is preferentially aligned normal to the fission axis. The de-excitation sequence preceding the $2^+ \rightarrow 0^+$ transition and the extra nuclear effects could only disperse the original nuclear alignment, so that independent of any model one assumes for the de-excitation process, the original

angular momentum was aligned preferentially perpendicular to the fission axis. A calculation of the population of the various m substates of the 2^+ level was obtained from analysis of the statistical de-excitation process using Eqs. 4 and 5 and assuming complete alignment before the de-excitation process. The results for an initial value of B = 6 are shown in Fig. 9 and are in good agreement with the experimental results. Therefore the observed magnitude of the alignment of the 2^+ level is consistent with an initial angular momentum comparable to that obtained from analysis of the gamma ray intensity measurements.

The two general methods used to determine the magnitude of the angular momentum yielded somewhat different results. The statistical model analysis for ^{144}Ba gave a value of B = 7.2 (a rms value of ℓ = 6.7) where the reaction comparison results implied an average angular momentum for this nucleus of ℓ = 9.2. The discrepancies between the methods can be attributed, on one hand, to inadequacies in the assumptions of the statistical model analysis used and, on the other hand, in the case of the reaction comparisons, possibly to the "resolution" available for interpolating such a wide variety of experimental data and also to differences in the actual population distribution of the angular momentum in fission and (charged particle, xn) reactions. Therefore the absolute uncertainty of the determination of the magnitude of the angular momentum is implied by these discrepancies. However, the variation of the angular momentum as a function of products is essentially independent of the method of analysis as long as the supposition is valid that the intensities of the transitions in the ground-state band reflect the primary angular momentum distribution.

IV. Kinetic Energy Effects

The experimental results have also been used to study the effects of fragment kinetic energy on the primary angular momentum of the fission products. For the formation of the same primary fission fragments the total energy release, Q, of the fission process is fixed and can be considered as the sum of the kinetic energy of the products, E_K, and their internal excitation energies, E_x:

$$Q = E_K + E_x$$

Therefore it is seen that for a fixed Q the events with high relative kinetic energy are those having low internal excitation energy. One consequence of this is that since the internal energy is primarily dissipated through the evaporation of neutrons, fragments with higher kinetic energy will have low internal energy and therefore evaporate fewer neutrons. An example is shown in Fig. 10 which presents a portion of a gamma ray spectrum for three total kinetic energy release intervals. The indicated peaks are the $2^+ \rightarrow 0^+$ ground state transitions of three adjacent even-even Ru isotopes; 108, 110 and 112. If the three spectra were summed the photo peak height would be representative of the fission yields of these isotopes. Since the total Q value for the formation of adjacent isotopes is reasonably constant the relative yields of these transitions in the three spectra reflect the neutron evaporation probabilities as a function of kinetic energy. It is seen that the heaviest Ru isotope has its highest yield in the high kinetic energy interval while the transition from the lightest Ru isotope, which appears as a shoulder relative to ^{110}Ru in the high

kinetic energy interval, is the dominant peak in the low kinetic energy interval. We interpret these yields as supporting the contention that the heaviest Ru isotope has had the lowest internal excitation energy and has evaporated the fewest neutrons and conversely the lightest Ru isotope is associated with the lower kinetic energy and has had the highest internal energy and has evaporated the most neutrons.

There is therefore a strong correlation in fission product yield with total kinetic energy release in fission. We have also studied the correlation between fragment angular momentum and kinetic energy release. The relative intensities of the ground state band transitions as a function of three kinetic energy intervals (low 150 - 180 MeV, medium 180 - 190 MeV, high 190 - 225 MeV) are presented in Table 4. The data were obtained by sorting the γ-ray spectra according to both mass and kinetic energy. For each line a relative intensity was obtained in those mass intervals where significant data were available. The experimentally determined relative intensities of $4^+ \rightarrow 2^+$ and $6^+ \rightarrow 4^+$ transitions in each E_K interval were divided by the $2^+ \rightarrow 0^+$ relative intensity in that interval. The results are finally presented by normalizing the ratio of $E_{I \rightarrow I-2}/E_{2^+ \rightarrow 0^+}$ (I=4,6) to unity for the medium interval of E_K (180 - 190 MeV). In this way the results are independent of detector efficiency. For several isotopes results were obtained in two independent experiments utilizing two different geometries and different Ge(Li)detectors (the experimental data labeled HR were obtained with a 1 cc detector and those labeled GX were obtained with a 6 cc detector). The mean deviation between results of the two

experiments for a given isotope is 0.10 which is an indication of the uncertainty of the experiment. On the whole there is perhaps a tendency of slightly higher ratio for the light fragments. A higher ratio implies relatively higher feeding of high angular momentum states and consequently higher angular momentum.

A 15% change in the ratio $I_{4+\rightarrow 2+}/I_{2+\rightarrow 0+}$ corresponds, according to the statistical model calculation, to a change of ~ 2 units in the initial angular momentum. In such a case a larger change should be observed in the $I_{6+\rightarrow 4+}/I_{2+\rightarrow 0+}$ ratio. As this is not observed in the experiment the conclusion is that the value of J is on the average (within ±1 units) independent of the fragment total kinetic energy. This result should be compared with the clear dependence of yields of the isotopes on the total kinetic energy, e.g. ^{112}Ru shows a change in relative yield of factor ~ 50 between the high and the low kinetic energy intervals.

V. Discussion

The variations in the primary angular momenta are presented in Fig. 11 using values derived from the statistical model analysis (Eq. 3). The data are plotted as a function of Z and each experimental point represents the average of the parameter B as determined from the various measured isotopes of that element (Table III). The graph is presented such that complementary elements lie on the same abscissa. The most obvious features presented in Fig. 11 are: (1) the variation in angular momentum between products is not large; (2) the heavy fragments have a somewhat greater angular momentum than the light fission products; (3) the angular momentum appears to decrease slightly for both the light and heavy fission fragment groups as symmetric division is approached.

An important feature to note is that the angular momentum does not correlate with the internal excitation energy of the products. The multiplicity of neutron evaporation by fission products is usually interpreted as a measure of the amount of internal excitation or deformation energy they possess. Figure 12 presents a plot of the neutron multiplicity[29] and of the angular momentum distributions as a function of atomic number. Whereas the neutrons show the well known "saw-tooth" behavior with the highest multiplicity occurring at Z=48, the angular momentum distribution is not in phase with this behavior. In fact, the fragments evaporating the largest number of neutrons have essentially the lowest primary angular momentum.

We have noted in previous publications that the lightest fission products (Mo and Zr) as well as the heaviest fission products (Ce, Nd, Sm) are apparently permanently deformed in their ground states.[18-20] With this knowledge it is possible to seek a correlation of the angular momentum with the amount of ground state deformation. We wish to see if the magnitude of the intrinsic quadrupole moment in a residual nucleus correlates with the average angular momentum of the fragment. The quadrupole moments of the primary fission products were calculated from the variable moment of inertia model of Mariscotti et al.[33] using the known experimental energies of the members of the ground state bands. The results of these calculations are presented in Table V. The implicit assumption is that the quadrupole moment of the primary fragment is the same as if the average angular momentum was present in the ground state band.

Figure 13 presents a plot of the data presented in Table V. The line is a non-weighted least squares fit to the seven more accurately known experimental points. It is seen that there is a reasonably good correlation with none of the better known points having a deviation of over 10% from the fitted line. The two remaining points have a larger deviation from the line (Z = 48 is 31%, Z = 62 is 15%) but since these points are known with less accuracy these deviations may not be significant. This correlation emphasizes the discrepancy between the liquid drop "deformation energy" (which is largest for Z = 46 and 48) and the magnitude of the angular momentum.

To summarize, the general experimental conclusions are that there are apparently only moderate deviations in the fragment angular momentum. This is seen in our current studies in which the product angular momentum as a function of element varied by less than a factor of two and that the deviation in angular momentum as a function of kinetic energy was only ~1-2 $\hbar$. From the previous studies of Sarantities, Gordon, and Coryell[16] there is also only ~1-2 $\hbar$ deviation in the product angular momentum for cases in which the fissioning compound nucleus is produced with varying excitation energy and angular momentum. The majority of the angular momentum of the compound nucleus goes into orbital angular momentum of the separating products instead of intrinsic fragment angular momentum. It should be pointed out that even for the spontaneous fission of ^{252}Cf which has an angular momentum of zero the products do not have to have identical and cancelling angular momentum. Whatever deviations that do exist between the two primary products can be made up by orbital angular momentum of the system.

In the discussion to follow we argue that these results are consistent with the quasi statistical equilibrium at scission model[2] in which (1) there is an approximate constancy in neck width at the scission point (here defined as the point at which the nuclear matter density on the axis of the thinnest portion of the neck has fallen to half the central nuclear density) and (2) there is only a relatively minor role for post-scission Coulomb excitation.

We had expected that the average angular momentum might show a positive correlation with $\bar{\nu}$, the average number of neutrons emitted, but such a correlation is clearly absent. Either of two models (A and B) would lead to such a correlation. The quantity $\bar{\nu}$ is generally assumed to be a measure of the shape distortion energy at scission, hence the higher $\bar{\nu}$ the more distorted is the fragment.

Model A would assume near scission some sort of equilibration of energy among collective degrees of freedom (though not among all degrees of freedom). It would further assume that the rotational moment of inertia increased with distortion. Various rotational angular momentum states would then be populated according to a Boltzmann factor of some appropriate "temperature" for the collective modes. Clearly, the more distorted the fragment, the more rotational angular momentum it would receive on the average.

$$|a_I|^2 = (2I + 1) \exp\left[-\frac{\hbar^2}{2\mathcal{J}} I(I + 1)/\theta\right] \qquad (7)$$

Model B would focus attention on the zero-point motion in the bending and wriggling modes at scission. Treatment of related cases has been made by Nix and Swiatecki[1] and by Rasmussen, Mang, and Nörenberg.[2] The former authors treated symmetric division of nuclei in the region of astatine, where saddle and scission points are sufficiently close that

statistical equilibrium at scission is justified. The latter authors treated the case of asymmetric division of heavy elements in the idealized situation of one fragment (in the ^{132}Sn region) remaining spherical. These models are appealing because of the very few adjustable parameters. The harmonic potential essentially depends only on curvature of the touching tips, fragment charges, and the center to center distance of the fragments. Reasonable estimates of fragment moments of inertia can be made. The greater tip curvature and increasing moment of inertia that go with increasing distortion cause a decrease of the Gaussian zero-point amplitude b in the bending mode. The fragment angular momentum distribution just after scission may be taken from expansion of the wave function in symmetric-top rotor functions; hence, the narrower the zero-point angular wave packet the larger the average angular momentum.

$$a_I = \int_0^{\pi} e^{-\frac{\beta^2}{2b^2}} \left(\frac{2I+1}{2}\right)^{1/2} P_I(\cos\beta) \sin\beta \, d\beta$$

$$\approx \text{Const.} \times (2I+1) \exp\left[-(I+1/2)^2/b^2\right] \qquad (8)$$

Nix and Swiatecki arrived at angular momentum distributions in a formally different way, but one that is equivalent. They used the zero-point coordinate and momentum distributions as a starting point for integration of the classical equations of motion of the separating fragments. Their calculations on symmetric fission of excited ^{213}At using the touching spheroids at scission predicted a most probable value for I of 15 $\hbar$ if the spheroids had infinite viscosity and were "frozen" into their deformed shapes. They predicted a most probable value for I of 8.5 $\hbar$ if the electrostatic interaction between fragments were zero. The difference

of these two calculations represents in their mode the maximum effect possible for post-scission Coulomb excitation.

From the general magnitude of our observed I values in ^{252}Cf compared with the two cases of Nix and Swiatecki we would infer a minor role for Coulomb excitation. Secondly, if fragments were very viscous and Coulomb excitation became important, the $I_{ave.}$ values should then correlate with $\bar{\nu}$, and we have seen they do not.

We may rescue model B only by assuming that the zero-point vibration amplitudes that go over into rotation are practically constant for all degrees of mass asymmetry in division. Perhaps the zero-point uncertainty of fragment tips with respect to the center-to-center axis is a distance about equal to the diffuseness of the nuclear surface. Certainly it cannot be less.

From Eq. 8 we can calculate the average spin

$$I_{ave.} = \sum_{I=0}^{\infty} I|a_I|^2 \Big/ \sum_{I=0}^{\infty} |a_I|^2 \approx \frac{\sqrt{\pi}}{2b} - 1/2. \qquad (9)$$

Let us make some estimates. The r.m.s. average I is about the reciprocal of b. At scission a first estimate of b is the angle subtended by the nuclear surface diffuseness length at the distance of the neck from the center of mass of the fragment. For surface diffuseness length we take the parameter a_o in the Fermi density function

$$\rho_F(r) = \rho_o[1+\exp[(r-c)/a_o]]^{-1}$$

Experimentally a_o is around 0.5 - 0.6 Fm. The simple Coulomb energy estimate of center-to-center scission distance in ^{252}Cf is around 17Fm. On this basis the neck is about 8.5 Fm from the centers and the angular width b of the bending wave packet would be 1/15 radian. This answer is too small by a factor of two, and we consider alternatives. For the neck density

to fall off as rapidly with radial distance as the density falls from half density in the nuclear surface is unreasonable, since that implies unusually high kinetic energy of the nucleons in the neck region. For an orbital at the Fermi energy of 40 MeV in the neck region let us neglect energy associated with motion along the Z-axis. Thus, we consider the width of the Gaussian zero-point motion in the two-dinensional harmonic potential across the neck. The characteristic oscillator energy $\hbar\omega$ will be 40 MeV and the zero-point amplitude is $\sqrt{\frac{\hbar}{m\omega}} \approx 1.0$ Fm. This width gives a reasonable angular packet of 1/8.5 radians. A third estimate would consider that the nuclear potential is not at its full central depth at the scission neck. Perhaps, then the wave packet will not be narrower than the r.m.s. radius of the alpha particle, which is 1.6 Fm. This width gives the most reasonable value of scission r.m.s. angular momentum 5.3 ($= \frac{8.5 \text{ Fm}}{1.6 \text{ Fm}}$).

We feel that we now can qualitatively interpret these results in a consistent manner in terms of the universal neck size for all scission splits. That the lightest and heaviest fragments have somewhat larger $I_{ave.}$ than the others may mean that Coulomb excitation does add another 2-4 units of average angular momentum where the ground states of the fragment have stable deformed shapes.

Is there any special significance to the observation that complementary fragments have near equal $I_{ave.}$ values? We think not. The conservation of angular momentum requires that three vectors, the angular momenta of the fragments and the orbital angular momentum of the system sum to zero after separation but before neutron emission.

Because the inertial parameter $\frac{A_1 A_2}{A_1+A_2} r_{12}^2$ for orbital motion is always much larger than the moments of inertia of the two fragments,

conservation of angular momentum will not pose a serious constraint on the fragment angular momenta. The fragment angular momenta can be governed, as discussed above, by their angular wave packets at scission, and the orbital angular momentum of the system adjusts to satisfy overall L conservation.

It is not clear that we have much to gain now by further refinements in the theory. The Nix-Swiatecki vibrational normal-mode calculations could be generalized to unequal mass division and to more realistic shapes than touching spheroids. The Rasmussen, Nörenberg, Mang model could be generalized to both fragments deformed. The restoring force for angular rocking acts as a spring between centers of curvature of the two tips. Thus, the general problem can be reduced to the problem of two two-dimensional isotropic harmonic oscillators with harmonic coupling. The bending and wriggling normal modes then separate in this formulation. The zero-point wave functions can finally be expended in products of symmetric top rotor functions for the fragments. It does not seem worthwhile here to refine model B to this extent, for it has been argued[34] that for the heaviest elements the scission point is so far from saddle point that the statistical picture, equilibrating energy among various modes of motion, does not apply and one must solve the detailed dynamics of motion from saddle to scission. We would like to hope that the statistical approach at scission still retains validity in the sense that the system will tend to adiabatically minimize the energy tied up in the bending modes, so long as their potential and inertial parameters do not sharply change on the path from saddle to scission.

We have carried out additional calculations of Coulomb excitation for cases of fixed deformation. These calculations are described in the Appendix, and they support the conclusion that Coulomb excitation only slightly alters the angular momentum distribution at scission.

ACKNOWLEDGMENTS

We wish to acknowledge helpful discussions on many aspects of this paper with Drs. L. G. Moretto, W. D. Myers, G. Struble, W. J. Swiatecki and C. F. Tsang.

Appendix

Calculation of Coulomb-Excitation Effects.

We observe that there is no correlation between average angular momentum of fragments $< \ell >$ and their scission-point deformation, as inferred from average number of neutrons $\bar{\nu}$. There seems, however, to be some correlation between $< \ell >$ and the ground band deformation of the fragments. This correlation would indicate to us the need to examine carefully the possibility of significant Coulomb excitation effects after scission. A number of calculations of Coulomb excitation effects have been made. The additional angular momentum thus coming in the post-scission period depends greatly on assumptions about the time behavior of the fragment shapes. If the prolate fragments maintain most of their deformation, the Coulomb excitation effects can be large. If the fragments undergo quadrupole shape vibrations, either damped or undamped, Coulomb excitation effects are small. Despite the above qualitative understanding afforded by previous calculations, we felt it of value to reformulate and study the fission Coulomb excitation problem in the light of the new data.

Rasmussen and Sugawara-Tanabe[35] have given a WKB method of calculating multiple Coulomb excitation in the limit of infinite moment-of-inertia. The phase shift due to the quadrupole potential is calculated in the one-dimensional radial wave equation with potential energy that obtaining for a spherical nucleus along the line of the symmetry axis of a spheroidal nucleus.

In treating the mutual Coulomb excitation of fission fragments we shall restrict ourselves to the quadrupole-monopole interaction, ignoring quadrupole-quadrupole or higher order interactions with their shorter range nature. Furthermore, we ignore effects of the nuclear potential and neglect

rotational energy. As with alpha decay of spin-zero nuclei the problem may be solved in the nuclear frame $\theta'\psi'$. Thus, the Hamiltonian is

$$H = -\frac{\hbar^2}{2\mu}\nabla^2 + \frac{Z_1 Z_2 e^2}{r} + \frac{Z_1 Q_2 e^2}{2r^3} P_2(\cos\theta'), \qquad (A.1)$$

where θ' is the angle of the symmetry axis of fragment 2 with respect to the line of centers, μ is the reduced mass, and Q_2 is the intrinsic quadrupole moment of fragment 2. The presence of the quadrupole interaction term displaces the classical turning radius, and Coulomb excitation matrix elements may be approximated by evaluating the resulting shift in phase at infinite radius for the regular solutions of the wave equation.

By Fröman's[36] approximation for the three-dimensional wave equation the solution for a single ℓ-value at its turning radius is continued out to large distance by solving the one-dimensional wave equation along constant θ' rays.

Thus, invoking also the WKB approximation we get the asymptotic wave function

$$\psi(r,\theta',\phi') = Y_{\ell m}(\theta',\phi') \exp[i\int_{r_\ell}^{r} k_\ell dr + i\,\pi/4] \qquad (A.2)$$

Where $$k_\ell = \frac{1}{\hbar}\left\{ 2\mu[E - \frac{Z_1 Z_2 e^2}{r} - \frac{\hbar^2}{2\mu r^2}\ \ell(\ell+1) - \frac{Z_1 Q_2 e^2}{2r^3} P_2(\cos\theta'] \right\}^{1/2}$$

We designate $k_\ell^{(0)}$ as the corresponding wave number without the quadrupole term. Also $r_\ell(\theta')$ and $r_\ell^{(0)}$ are turning radii with and without quadrupole interaction.

Without the quadrupole term the phase factor is just the Coulomb phase factor

$$\sigma_c = \mathrm{Arg}\,\Gamma(\ell + 1 + i\eta) \quad \text{with } \eta = \frac{Z_1 Z_2 e^2}{\hbar v}$$

Thus, the Fröman matrix elements are found by projection from the asymptotic wave function

$$k_{\ell\ell'm} = \lim_{r\to\infty} \int Y^*_{\ell'm}\, \psi(r,\theta',\phi') \cdot e^{-i\sigma_c}\, dw$$

$$= \int Y^*_{\ell'm} \exp\left[i\int_{r_\ell}^{\infty} k_\ell^{(\theta')}\, dr - i\int_{r_\ell(0)}^{\infty} k_\ell^{(0)} dr\right] Y_{\ell m}\, dw$$

$$= \int Y^*_{\ell'm} \exp[-i\,\delta_{\ell CE}]\, Y_{\ell m}\, dw. \qquad (A.3)$$

The Appendix of Ref. 35 outlines the method of evaluation of the Coulomb excitation phase shift $\delta_{\ell CE}$ in terms of elementary integrals.

We shall be concerned only with $m = 0$ waves, so

$$k_{\ell\ell'} = \int Y^*_{\ell 0} \exp[i\delta_{CE} P_2(\cos\theta')]\, Y_{\ell' 0}\, dw \qquad (A.4)$$

If the expansion coefficients of the angular wave function at scission are $a_{\ell'}$, then the amplitudes at infinity b_ℓ are given by multiplication by the Fröman matrix.

$$b_\ell = \sum_{\ell'} k_{\ell\ell'}\, a_{\ell'} \qquad (A.5)$$

It is commonly assumed that the angular wave function at scission must be some sort of peaked function, such as, a Gaussian in θ' or $\sin\theta'$ [(cf. Ref. 2 Eqs. (10) and (13)].

$$\psi_{sc} = e^{-\frac{\theta'^2}{2\gamma_0^2}} \qquad (A.6)$$

Thus,

$$a_{\ell'} = \int e^{-\frac{\theta'^2}{2\gamma_0^2}}\, Y_{\ell' 0}\, dw \qquad (A.7)$$

$$= \text{Const.} \cdot (2\ell'+1)\, \gamma_0^2 \exp\left[-(\ell+1/2)^2\gamma_0^2\right]$$

We can alternatively derive an expression directly for the amplitudes b_ℓ without the intermediary Fröman matrix.

$$b_\ell = \int_0^{2\pi} \int_0^{\pi} Y_{\ell o}(\omega') \exp[-\frac{\theta'^2}{2\gamma_o^2} - i\,\delta_{CE}\,P_2\,(\cos\theta')]\,dw' \quad (A.8)$$

We have numerically evaluated these integrals for various parameter sets comparable to fissioning nuclei. The resulting probability destributions $|b_\ell|^2$ were found in all cases to be very close to the standard form $|b_\ell|^2 \simeq (2\ell+1)\exp[-(\ell+1/2)^2\gamma_\infty]$.

Table A 1 gives the results of numerical integrations of Eq. (A.8) (with the quadrant 0 to $\pi/2$ subdivided into 60 intervals and the ordinary Simpson's rule used, ℓ values 0 through 18 being evaluated). The center-of-mass energy was taken as 200 MeV in all cases Z_2, A_2, and Q_2 refer to the charge, mass, and intrinsic quadrupole moment of the fragment being Coulomb excited. Z_1 and A_1 refer to the complementary fragment. The calculations are carried out for several values of γ_o^2, the mean square angular width of the rotational wave packet at scission according to Eq. (A.6). In the last column is the final average angular momentum according to Eq. (14) of Ref. 2. The differences of final average angular momentum with and without Coulomb excitation are small, even for the last case of unrealistically large quadrupole moment of 15.1 barns.

We have checked that these results are consistent with the classical formula of Eq. (15) of Ref. 2, if we take into account that a factor $\sqrt{Z_B}$ was erroneously omitted from the denominator of that expression. It should read

$$\Delta\ell = \left(\frac{e^2 MZ_A}{2Z_B}\right)^{1/2} \frac{Q_B \sin\gamma_o \cos\gamma_o}{\hbar\,\sigma^{3/2}} \tag{A.9}$$

where we have also replaced γ_o by $\sin\gamma_o \cos\gamma_o$. Here γ_o is the angle between the cylindrical symmetry axis and the center-to-center vector and σ_c is the classical turning radius. The average angular momentum change due to Coulomb excitation does not simply add to the average angular momentum at scission, as we shall see by an approximate analytical integration of Eq. (A.8).

Provided $\gamma_o^2 \ll 1$ so as to confine the main integrand to small angles, and provided ℓ is not too small, we can substitute the asymptotic expression for the spherical harmonic as follows:

$$Y_{\ell o}(\omega') = \sqrt{\frac{2\ell+1}{4\pi}}\; P_\ell(\cos\theta) \approx \sqrt{\frac{2\ell+1}{4\pi}}\; J_o[(\ell+1/2)\theta]$$

where J_o is as ordinary Bessel function. Since the integral mainly comes around $\theta = 0$, with an equal contribution (even ℓ) around $\theta = \pi$, we can put the upper limit at infinity and double the result. We also approximate $\sin\theta$ by θ

$$b_\ell \approx \sqrt{\pi(2\ell+1)} \cdot 2\int_0^\infty J_o[\ell+1/2]\,\exp\left[-\frac{\theta^2}{2\gamma_o^2} - i\,\delta_{CE}(1-3/2\,\theta^2)\right]\theta d\theta$$

$$= 2\cdot[\pi(2\ell+1)]^{1/2} e^{-i\delta_{CE}} \int_0^\infty J_o[\ell+1/2]\,\exp[-\alpha\theta^2]$$

$$\text{with } \alpha = \frac{1}{2\gamma_o^2} - i\frac{3}{2}\,\delta_{CE}$$

We find from integral tables that the integral has the value $\frac{1}{2\alpha}\exp[-(\ell+\frac{1}{2})^2/4\alpha]$.

Hence,

$$|b_\ell|^2 \approx \frac{(2\ell+1)\pi}{|\alpha|^2}\exp\left[-\frac{(\ell+1/2)^2}{4}\left(\frac{1}{\alpha}+\frac{1}{\alpha^*}\right)\right] = \frac{(2\ell+1)\pi}{|\alpha|^2}\exp\left[-\frac{(\ell+1/2)^2}{4|\alpha|^2\gamma_o^2}\right] \tag{A.11}$$

For parameters encountered in fission the Coulomb excitation phase shift δ_{CE} will not depend very much on ℓ, so we may as well use the simple expression for $\ell = o$ as used in Ref. 35.

$$\delta_{CE} = 1/3(2M_rE)^{1/2}\Delta r_t/\hbar \tag{A.12}$$

with E the kinetic energy, M_r the reduced mass, and r_t the displacement of the classical turning point at $\theta = o$ due to the quadrupole potential. To lowest order in the intrinsic quadrupole moment $\Delta r_t = Q_B/Z_B\sigma$.

If in Eq. (A.12) we substitute also for E the following

$$\delta_{CE} = 1/3\left(\frac{2\ M\ Z_A e^2}{Z_B}\right)^{1/2} \frac{Q_B}{\sigma^{3/2}} \tag{A.12a}$$

The correspondence of (A.12a) with the classical formula (A.9) is obvious. Formulas (A.11) and (A.12) give results very close to those of the numerical integration. Since Coulomb excitation only affects the angular momentum distribution through $|\alpha|^2 = (\frac{1}{4\gamma_o^4} + \frac{9}{4}\delta_{CE}^2)$, it only becomes significant as the second term becomes comparable to the first term in the $|\alpha|^2$ sum.

Under special forms of the angular wave packet at scission the Coulomb excitation could become more significant. Conceivably the second-saddle-point fission barrier could be unstable with respect to the lower symmetry bending displacement of the neck, just as it is unstable with respect to mass asymmetric displacements. In such a situation the angular packet at scission might not be a Gaussian centered on $\theta = o$ but could be of form

$$\psi_{SC} = \theta^{2n}\ e^{-\frac{\theta^2}{2\gamma_o}} \qquad \text{with a positive integer.} \tag{A.13}$$

This function has a maximum at $\theta = \sqrt{2n}\ \gamma_o$. In this case we can also

derive an approximate expression similar to Eq. (A.11). Here the integral in (A.10) becomes

$$\int_0^\infty J_0[(\ell+1/2)\theta]\ \exp\ [-\alpha\theta^2]\ \theta^{2n+1}\ d\theta.$$

This integral is equal to the following[37]

$$\int_0^\infty J_0[(\ell+1/2)]\ \exp[-\alpha\theta^2]\theta^{2n+1}d\theta = \frac{\Gamma(n+1)}{2\alpha^{n+1}}\ {}_1F_1\left[n+1;1;-\frac{(\ell+1/2)^2}{4\alpha}\right]$$

where the F function is a degenerate hypergeometric function. We have not made numerical studies with the boundary conditions of (A.13), but by the Correspondence Principle we would expect Eq. (A.9) to be a good approximation where we replace γ_0 in Eq.(A.9) by the angular maximum in (A.13), namely, $\sqrt{2n}\ \gamma_0$.

Other variants in the post scission Coulomb excitation problem mainly reduce the amount of Coulomb excitation. Secondly, if the prolate spheroidal scission shapes are unstable and there is oscillation toward spherical, the Coulomb excitation is reduced. However, the time for fragments to move from scission to where torque is halved is comparable to characteristic vibration times $1/\omega$ so the quadrupole shape vibration will not cause a large reduction below fixed-shape calculations.

FOOTNOTES AND REFERENCES

*Work performed under the auspices of the U. S. Atomic Energy Commission.

†Current address Weizmann Institute of Science, Rehovoth, Israel.

1. J. R. Nix and W. J. Swiatecki, Nucl. Phys. 71, 1 (1965).
2. J. O. Rasmussen, W. Nörenberg, and H. J. Mang, Nucl. Phys. A136, 456 (1969).
3. S. S. Kapoor and R. Ramanna, Phys. Rev. 133, B598 (1964).
4. M. M. Hoffman, Phys. Rev. 133, B714 (1964).
5. K. Skarsvåg and I. Singstad, Nucl. Phys. 62, 103 (1965).
6. K. Skarsvåg, Nucl. Phys. A96, 385 (1967).
7. G. Graff, A. Lajtai and L. Nagy in Proceedings of the Symposium on Physics and Chemistry of Fission, Salzburg, Austria, 1965 (International Atomic Energy Agency, Vienna, 1965), p. 163.
8. G. V. Val'skii, G. A. Petrov, and Yu. S. Pleva, Sov. J. Nucl. Phys. 5, 521 (1967).
9. G. V. Val'skii, G. A. Petrov, and Yu. S. Pleva, Sov. S. Nucl. Phys. 8, 171 (1969).
10. P. Armbruster, F. Hossfeld, H. Labus, K. Reichelt, in Proceedings of the Second IAEA Symposium on the Physics and Chemistry of Fission, Vienna, Austria, 1969 (International Atomic Energy Agency, Vienna, 1969), p. 545.
11. V. M. Strutinskii, JETP (Sov. Phys.) 10, 613 (1960).
12. S. A. E. Johansson and P. Kleinheinz, in Alpha, Beta and Gamma Ray Spectroscopy, edited by Kai Seigbahn, (North-Holland Publishing Company, Amsterdam, 1965) Vol. 1, p. 805.
13. T. D. Thomas and J. R. Grover, Phys. Rev. 159, 980 (1967).
14. I. F. Croall and H. H. J. Willis, J. Inorg. Nucl. Chem. 25, 1213 (1963).

15. H. Warhanek and R. Vandenbosch, J. Inorg. Nucl. Chem. 26, 669 (1964).

16. D. G. Sarantities, G. E. Gordon, and C. D. Coryell, Phys. Rev. 138, B353 (1965).

17. J. R. Huizenga and R. Vandenbosch, Phys. Rev. 120, 1305 (1960); R. Vandenbosch and J. R. Huizenga, Phys. Rev. 120, 1313 (1960).

18. E. Cheifetz, R. C. Jared, S. G. Thompson and J. B. Wilhelmy, Phys. Rev. Letters 25, 38 (1970).

19. J. B. Wilhelmy, S. G. Thompson, R. C. Jared, E. Cheifetz, Phys. Rev. Letters 25, 1122 (1970).

20. E. Cheifetz, R. C. Jared, S. G. Thompson, and J. B. Wilhelmy, in Proceedings of the International Conference on the Properties of Nuclei Far From the Region of Beta Stability, Leysin, Switzerland, 1970 (CERN, Geneva, 1970), Vol. 2, p. 883.

21. E. Cheifetz, J. B. Wilhelmy, R. C. Jared and S. G. Thompson. Phys. Rev. C, 4, 1913 (1971).

22. J. T. Routti and S. G. Prussin, Nucl. Instr. Methods 72, 125 (1969).

23. J. R. Huizenga and G. Igo, Nucl. Phys. 29, 462 (1962); Norman Glendenning, University of California Lawrence Berkeley Laboratory, private communication.

24. G. Bertrum Hansen, B. Elbeck, K. A. Hage-mann and W. F. Hornyak, Nucl. Phys. 47, p. 529 (1963).

25. J. O. Newton, F. S. Stephens, R. M. Diamond, K. Kotajima and E. Matthias, Nucl. Phys. A95, 357 (1967).

26. I. Bergström, C. J. Herrlander and I. Kerek, Nucl. Phys. A123, 99 (1969).

27. A. Luukko, A. Kerek, I. Rezanka and C. J. Herrlander, Nucl. Phys. A135, 49 (1969).

28. C. F. Williamson, S. M. Ferguson, B. J. Shepherd and I. Halpern, Phys. Rev. 174, 1544 (1968).

29. H. R. Bowman, J. C. D. Milton, S. G. Thompson and W. J. Swiatecki, Phys. Rev. 126, 2133 (1963).

30. J. M. Blatt and V. M. Weisskopf, Theoretical Nuclear Physics (John Wiley and Sons, New York, 1952)pp. 342-365.

31. J. O. Rasmussen and T. T. Sugihara, Phys. Rev. 151, 992 (1966).

32. S. R. de Goroot, H. A. Tolhoek and W. J. Huiskamp in Alpha, Beta, and Gamma Ray Spectroscopy, edited by Kai Seigbahn (North-Holland Publishing Company, Amsterdam, 1965), Vol. 2, p. 1199.

33. M. A. J. Mariscotti, Gertrude Scharff-Goldhaber and B. Buck, Phys. Rev. 178, 1964 (1969).

34. We gratefully acknowledge helpful discussions with V. M. Strutinskii and W. J. Swiatecki on this point.

35. J. O. Rasmussen and K. Sugawara-Tanabe, Nucl. Phys. A171, 497 (1971).

36. P. O. Fröman, Mat. Fys. Skr. Dan. Vid. Selsk., 1, (1965) No. 3.

37. I. M. Ryshik and I. S. Grodstein, Table of Series, Products and Integrals (Deutscher Verlag der Wissen Schaften, Berlin, 1957) section 6.631.

TABLE I. Angular distribution of specific transitions.

Isotope	E (keV)	γ Intensity (counts) 0°	22.5°	45°	67.5°	90°	$t_{1/2}$ nsec	a_2 and a_4 Fits a_2	a_4	a_2 Only a_2
						$2^+ \rightarrow 0^+$ Transitions				
^{100}Zr	213.0	665	876		602	450	0.52	.456 ± 0.088	0.559 ± 0.189	0.334 ± 0.175
^{102}Zr	152.0		1392	1494		1303	0.86			
^{104}Mo	192.6		2176	2076	1686	1636	0.45	0.269 ± 0.115	0.068 ± 0.215	0.274 ± .115
^{106}Mo	171.9	2670	2670	2450	2367	2456	0.75	0.065 ± 0.099	0.058 ± 0.151	0.083 ± 0.088
^{110}Ru	240.9	1392	1370	1005	1040	980	0.23	0.229 ± 0.101	0.195 ± 0.153	0.267 ± 0.096
^{144}Ba	199.5	1863	1819	1775	1503	1474	0.49	0.204 ± 0.097	-0.060 ± 0.153	0.187 ± 0.089
^{148}Ce	158.7	1862	1778	1527	1472		0.9	0.151 ± 0.182	0.113 ± 0.211	0.221 ± 0.126
						Other Transitions				
$^{(107)}Tc$	91.7	1477	1863	1700	1641	1514		0.077 ± 0.094	-.194 ± .138	0.094 ± 0.088
^{105}Mo	95.0	2360	3275	3537	4158	3824		-0.209 ± 0.093	-.204 ± .127	-.312 ± 0.078
^{101}Zr, ^{109}Ru	98.3	2175	2620	3190	4054	3735		-.320 ± 0.093	-.100 ± .128	-.372 ± 0.064
^{111}Ru	104.2	2332	2277	2139	2188	1846		.152 ± 0.095	-.058 ± .146	.138 ± 0.088
$^{(108)}Tc$	138.1	2909	2430	2730	2724	2890		-.080 ± 0.098	.106 ± .153	-.045 ± .084

TABLE II. Data for reaction comparison.

$\bar{\ell}$ ($\hbar$)	Reaction	Energy of Projectile (MeV)	Ref.
3	$^{159}Tb(p,2n)^{158}Dy$	12	a
8	$^{184}W(\alpha,2n)^{186}Os$	27	b
9.6	$^{126}Tc(\alpha,2n)^{128}Xe$	28	c
11	$^{116}Sn(\alpha,2n)^{118}Te$	33.5	d
13	$^{161}Dy(\alpha,3n)^{162}Er$	40.5	e
22	$^{159}Tb(^{14}N,5n)^{168}Hf$	93	b

a Ref. 24, b Ref. 25, c Ref. 26, d Ref. 27, e Ref. 28.

TABLE III. Derived values of the angular momentum parameter $\bar{B}$.

Isosope	Number of Levels Used for Determination	$\bar{\nu}$ [a]	$\bar{B}$ / $\hbar$	Weighted average [b] of $\bar{B}$ for each Element
^{100}Zr	2	1.81	6.15	
^{102}Zr	4	1.41	6.60	6.45
^{104}Mo	3	2.4	6.70	
^{106}Mo	3	1.8	5.80	6.25
$^{108,110}Ru$	4	2.8	5.50	
^{112}Ru	2	2.8	6.35	5.78
^{112}Pd	3	3.8	5.60	
^{114}Pd	3	3.6	5.40	4.82
^{116}Pd	2	3.2	2.80	
^{118}Cd	2	3.6	6.15	6.15
^{138}Xe	2	2.0	6.70	
^{140}Xe	2	1.0	10.05	8.37
^{142}Ba	3	2.0	8.20	
^{144}Ba	4	1.4	7.20	7.24
^{146}Ba	2	.9	5.90	
^{146}Ce	3	2.8	8.80	
^{148}Ce	3	1.9	8.90	8.87
^{150}Ce	3	1.2	8.90	
^{152}Nd	2	2.0	8.85	
^{154}Nd	3	2.5	9.75	9.39
^{158}Sn	3	2.8	11.1	11.1

a) The $\bar{\nu}$ values are the average number of neutrons emitted by the corresponding isotopes. These values are taken from the experimental results of Ref. 29 and have been corrected to be consistent with the results from Ref. 18-20.

b) The average has been weighted by the number of levels used for determination of $\bar{B}$ for each isotope of the element.

TABLE IV. Relative intensities of ground state band transitions for three kinetic energy intervals. See text for details.

Isotope	Exp.	$4^+ \rightarrow 2^+/2^+ \rightarrow 0^+$ Low (150-180 MeV)	Medium (180-190 MeV)	High (190-225 MeV)	$6^+ \rightarrow 4^+/2^+ \rightarrow 0^+$ Low (150-180 MeV)	Medium (180-190 MeV)	High (190-225 MeV)
^{100}Zr	HR	1.14	1.00				
	GX	1.29	1.00	1.23	1.37	1.00	0.85
^{102}Zr	HR	0.96	1.00				
	GX	1.17	1.00	1.04			
^{104}Mo	HR	1.14	1.00	1.04			
	GX	1.14	1.00	0.93	1.00	1.00	0.85
^{106}Mo	HR	1.13	1.00	0.93	1.00	1.00	0.84
	GX	1.14	1.00	0.95	1.13	1.00	0.84
^{108}Ru	GX[a]	0.96	1.00	0.97			
^{110}Ru	GX[a]				1.14	1.00	0.68
^{112}Ru	GX		1.00	0.70			
^{112}Pd	GX	1.37	1.00	1.24			
^{114}Pd	GX		1.00	0.84		1.00	1.33
^{116}Pd	GX		1.00	0.63			
^{138}Xe	GX	0.92	1.00	0.96			
^{140}Xe	GX		1.00	0.93			
^{142}Ba	GX	0.95	1.00	1.02	1.24	1.00	1.28
^{144}Ba	HR	1.12	1.00	1.09			
	GX	1.00	1.00	1.02	0.94	1.00	0.89
^{146}Ba	HR		1.00	1.06			
	GX		1.00	0.91			
^{146}Ce	GX	0.98	1.00				
^{148}Ce	HR	0.88	1.00	0.98			
	GX	1.10	1.00	1.07	1.15	1.00	1.17
^{150}Ce	HR	0.88	1.00	1.11	0.88	1.00	1.14
Average	All	1.07	1.00	0.98	1.10	1.00	1.00
	Light	1.15	1.00	0.95	1.16	1.00	0.91
	Heavy	0.97	1.00	1.05	1.05	1.00	1.12

[a] The $4^+ \rightarrow 2^+$ transitions in ^{108}Ru and ^{110}Ru could not be experimentally resolved and therefore have been ratioed to the combined $2^+ \rightarrow 0^+$ transition intensities of the two isotopes.

TABLE V. Average determined angular momentum of fission products ($\overline{B}$) and calculated quadrupole moments of ground state bands evaluated at $\overline{B}$.

Z	$\overline{B}$	Calculated Quadrupole Moments (barns)
40	6.45	6.47
42	6.25	5.70
44	5.78	5.47
46	4.82	4.70
48	(6.15)	(4.60)
56	7.24	6.40
58	8.87	7.33
60	9.39	8.66
62	(11.1)	(8.50)

TABLE A1. Post-Scission Coulomb Excitation Calculations.

Z_1	A_1	Z_2	A_2	Q_2	r_o^2	$J_{ave.}$
40	102	58	150	5.1	.05	2.82
40	102	58	150	0	.05	2.31
58	150	40	102	4.8	.01	6.01
40	102	58	150	0	.01	5.77
40	102	58	150	5.1	.01	5.80
40	102	58	150	5.1	.0167	4.40
40	102	58	150	0	.0167	4.30
40	102	58	150	15.1	.0167	5.18

Kinetic energy is taken as 200 MeV. Q_2 is in barns.

Fig. 1. Schematic representation of the experimental detector configuration. Detectors F_1 (with electrodeposited ^{252}Cf) and F_2 were used to measure the fragment kinetic energies. Detectors γ_1 and γ_2 measured energies of γ-rays and/or x-rays. The sources and detectors indicated at the bottom of the figure were used for external stabilization of the photon detectors.

Fig. 2. Experimental configuration for the angular distribution studies of the prompt fission gamma rays. The dashed line is the second location of the Ge detector thus allowing the angular distribution to be studied at 6 angles.

Fig. 3. Portions of gamma ray spectra recorded at three angles relative to the fission axis for the cases when light fission fragments have entered the Pt backings. The labeled transitions are associated with the indicated isotopes. Gamma rays from light fission products appear as sharp lines at all angles, however, gamma rays from heavy fission products (e.g. ^{144}Ba) are Doppler shifted and are recorded at varying energies depending on the angle of detection.

Fig. 4. Angular distributions of three prompt fission gamma rays relative to the fission axis. The lines represent least squares fits of the experimental data to Eq. 1.

Fig. 5. A schematic representation of the de-excitation of the fission fragments. The primary fragments can be visualized as tumbling as they separate. They possess ~15-20 MeV excitation energy which is predominantly dissipated through evaporation of neutrons. After neutron evaporation the remaining energy and angular momentum is removed by gamma ray transition. If the residual fission product is even-even the de-excitation

process will eventually strongly feed the ground state band. These intra-band gamma ray transitions are what are observed in the experiment.

Fig. 6. A comparison of the observed relative intra ground state band transition intensities from the current experimental results (triangles) with those observed in various charged particle, xn reactions (lines). The reaction data are labeled with the average angular momentum of the reaction as calculated from optical model codes. A tabulating of these data are presented in Table 2.

Fig. 7. The calculated angular momentum distribution for an initially formed fission product and for the residual products after evaporation of the first and second neutron. In the bottom portion of the figure the horizontal lines represent the location of the ground state band of the residual nucleus. The dashed line is an approximate "yrast" line calculated using a rigid body moment of inertia.

Fig. 8. The points are the observed ground state band transition intensities in the de-excitation of the fission product ^{144}Ba. The lines are a family of calculated transition intensities as a function of the angular momentum parameter B(Eq. 3). The calculations were performed using Eq. 4 and 5 with the experimental parameters indicated. σ_γ and σ_n are respectively the spin cutoff parameters associated with γ-ray emission and neutron evaporation and $\bar{\nu}$ is the average number of neutrons emitted.

Fig. 9. The points are the calculated populations of the various m substates of the 2^+ level in ^{144}Ba. These values were determined using the fitted experimental angular distribution of the $2^+ \rightarrow 0^+$ gamma ray. The solid line represents the predicted population of the m states as calculated

from the statistical model analysis of the de-excitation process using Eqs. 4 and 5 with an assumed value of B = 6 (Eq. 3) for the initial angular momentum distribution.

Fig. 10. Portions of prompt fission ganna ray spectra obtained for three intervals of total kinetic energy release. The labeled peaks are the $2^+ \rightarrow 0^+$ transitions in adjacent even-even Ru isotopes. The heaviest isotope, ^{112}Ru, has its highest yield, relative to other isotopes, in the high kinetic energy interval. Conversely the lightest isotope, ^{108}Ru, has its maximum relative yield in the low kinetic energy interval. These yields are interpreted to reflect the effects of internal excitation of the primary fragments. The fragments with the largest internal excitation energy evaporate the most neutrons and form the lightest products. Energy conservation requires that these products have the lowest total kinetic energy.

Fig. 11. A plot of the derived angular momentum parameter B [B≈rms(J)+1/2] as a function of atomic number. Each datum point represents an average of the parameter B as determined from various measured isotopes of that element (Table 3). The data in parentheses joined by dashed lines represents determinations from limited experimental data and are therefore taken to be less certain. The plot is presented such that complementary elements are on the same abscissa.

Fig. 12. A plot comparing the neutron multiplicity and angular momentum parameter (B) as a function of atomic number. The neutron multiplicity data show the well know "saw tooth" behavior, while no such effects are present in the angular momentum distributions of the products. It should be noted that fragments evaporating the largest number of neutrons have essentially the lowest angular momentum. The arrows indicate which ordinate values apply to the curves.

Fig. 13. A plot of the angular momentum (B) as a function of calculated quadrupole moment. Each point is labeled with the atomic number with which it is associated. The line represents the results of a least squares fit (excluding the two points in parentheses) to the experimental data points.

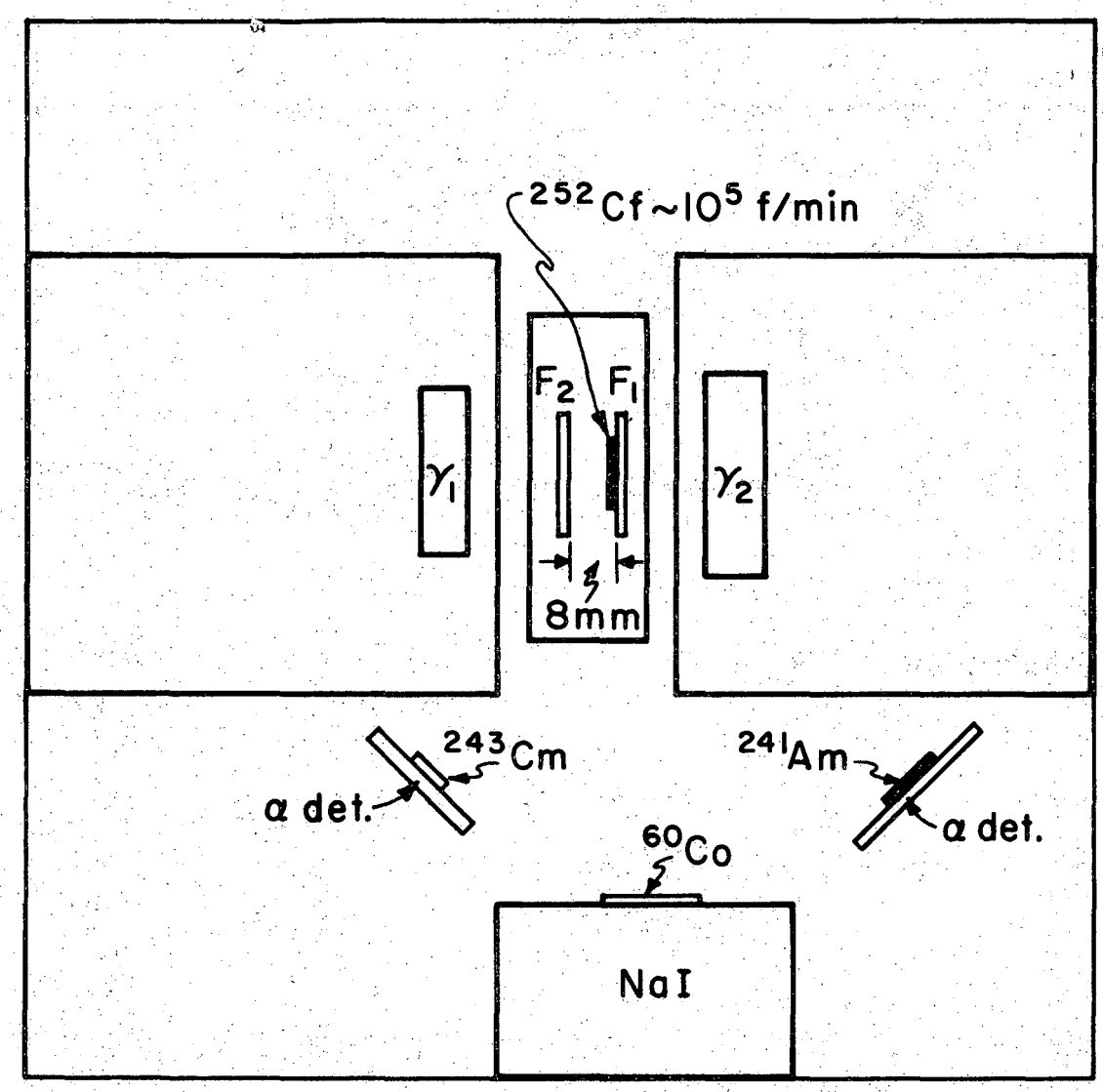

XBL703-2403

Fig. 1

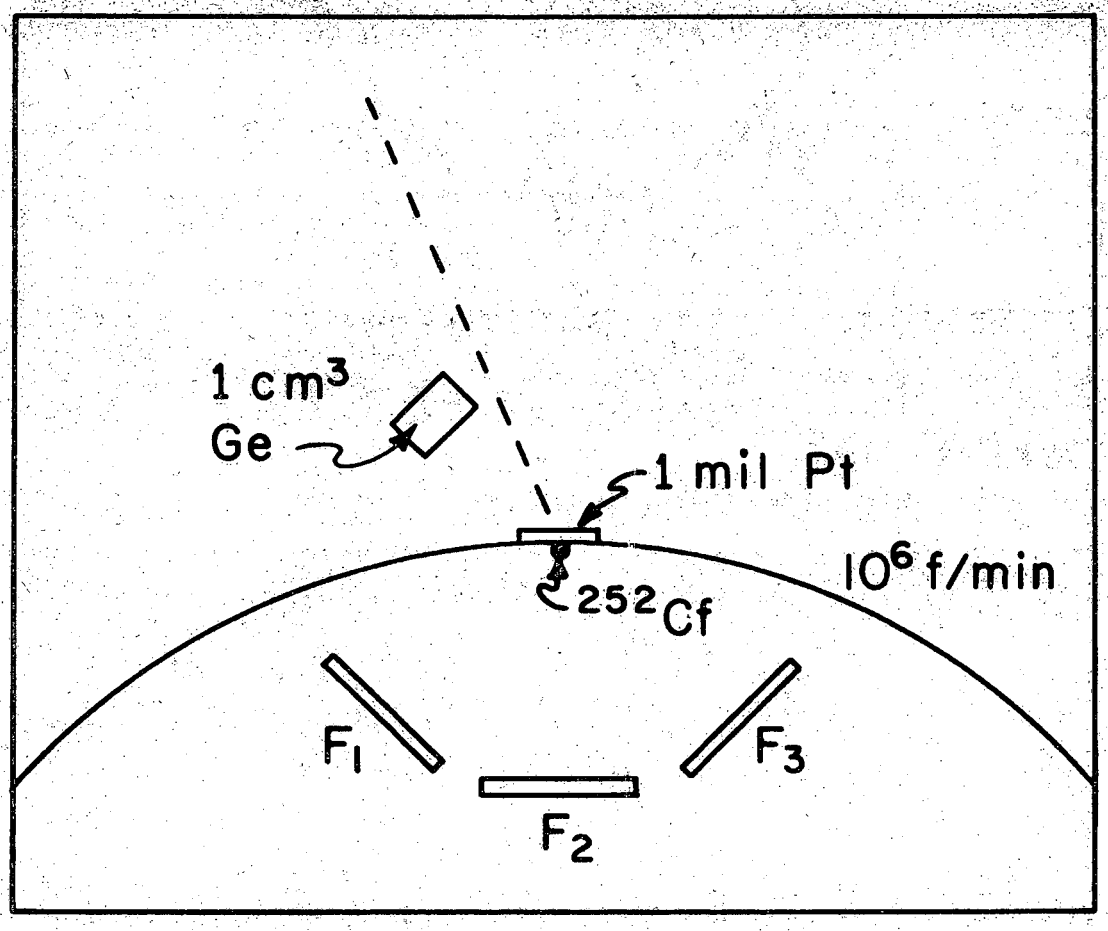

XBL703-2400

Fig. 2

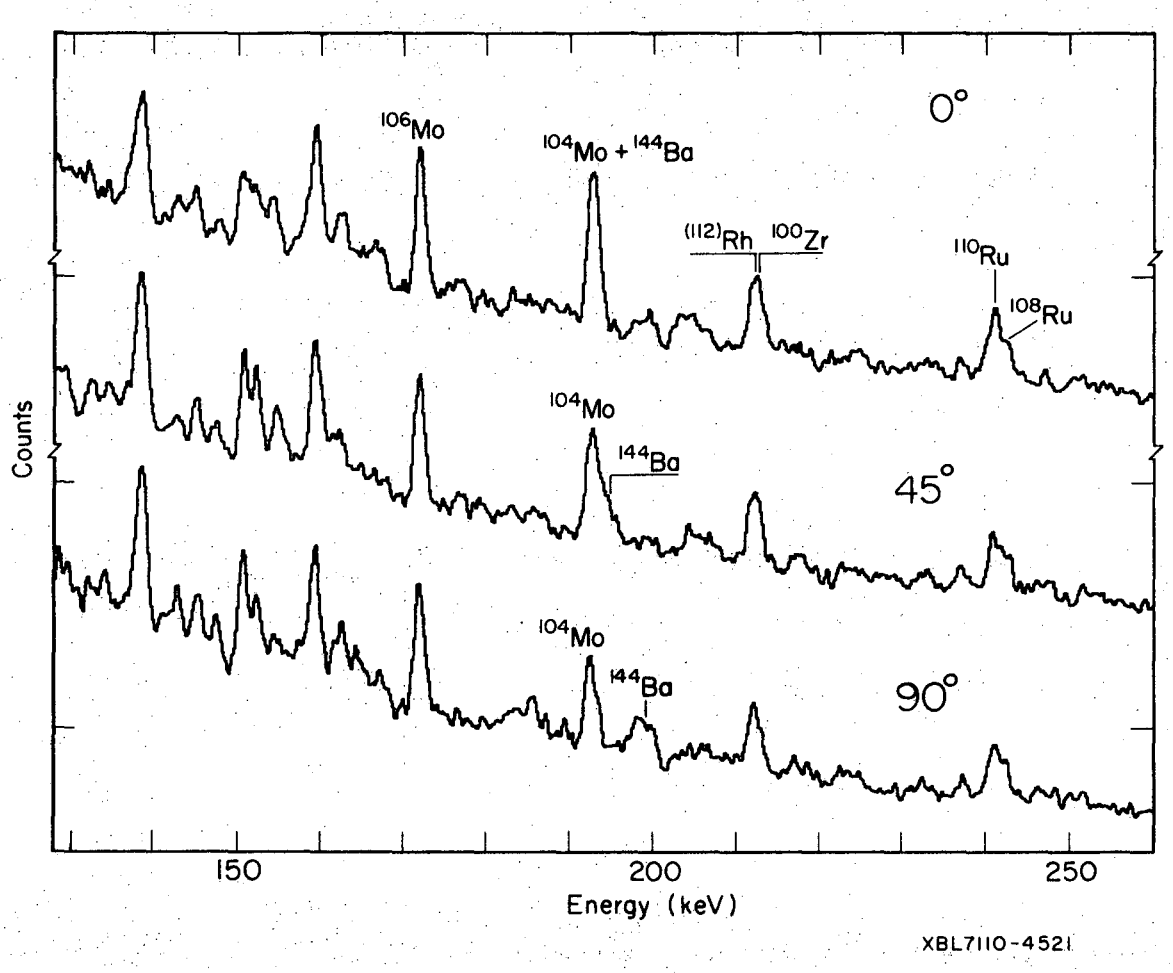
0°
45°
90°
106Mo
104Mo + 144Ba
(112)Rh
100Zr
110Ru
108Ru
104Mo
144Ba
104Mo
144Ba
Counts
150
200
250
Energy (keV)
XBL7110-4521

Fig. 3

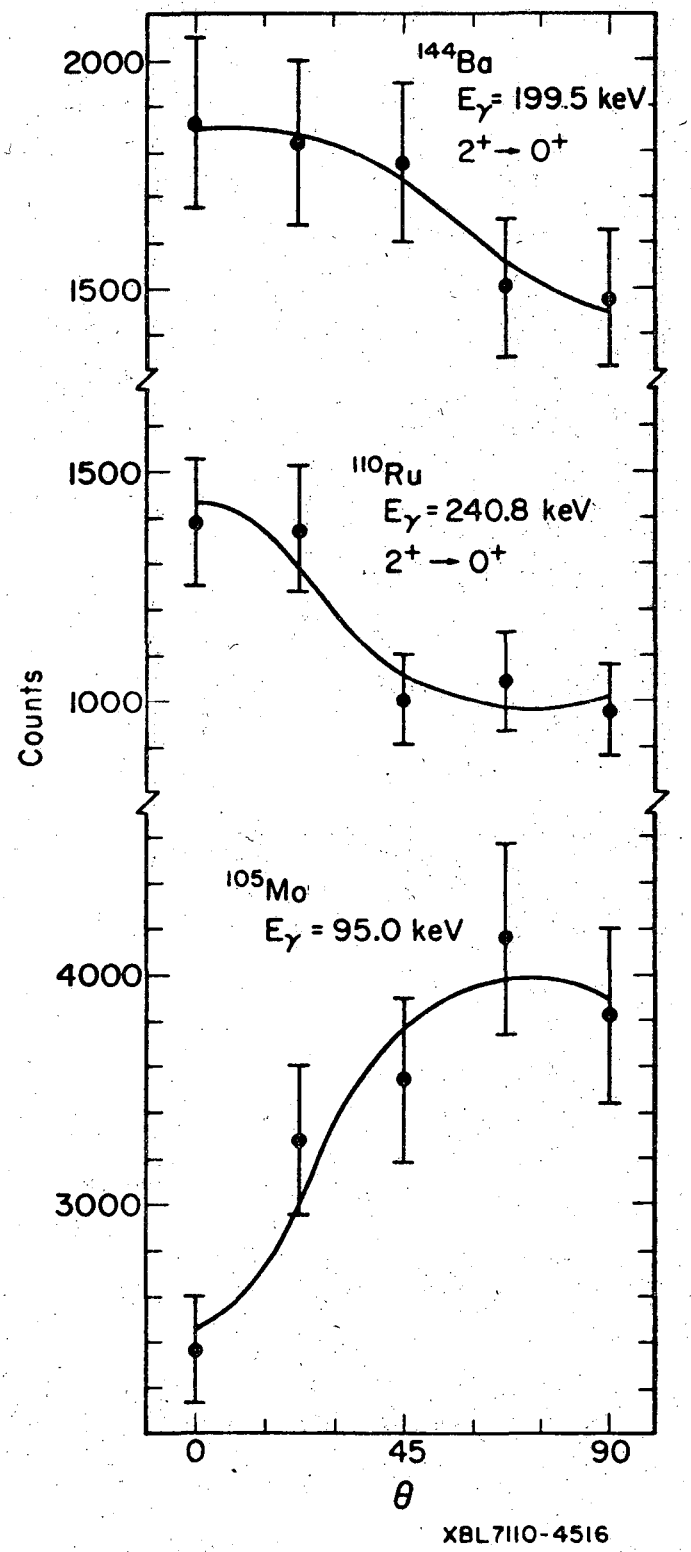
2000
1500
^{144}Ba
E_γ= 199.5 keV
$2^+ \rightarrow 0^+$
1500
1000
^{110}Ru
E_γ = 240.8 keV
$2^+ \rightarrow 0^+$
Counts
4000
3000
^{105}Mo
E_γ = 95.0 keV
0
45
90
θ
XBL7110-4516

Fig. 4

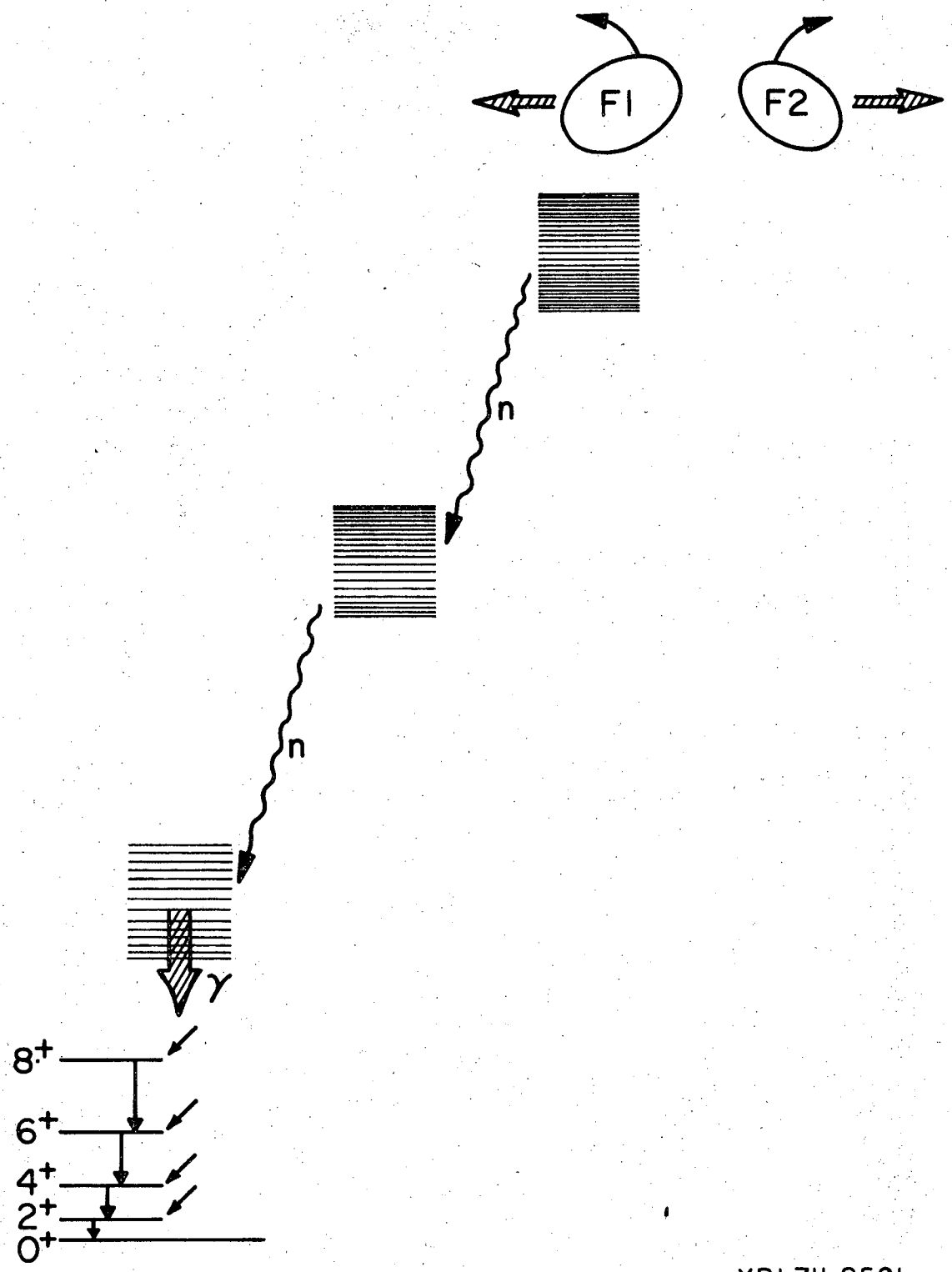

Fig. 5

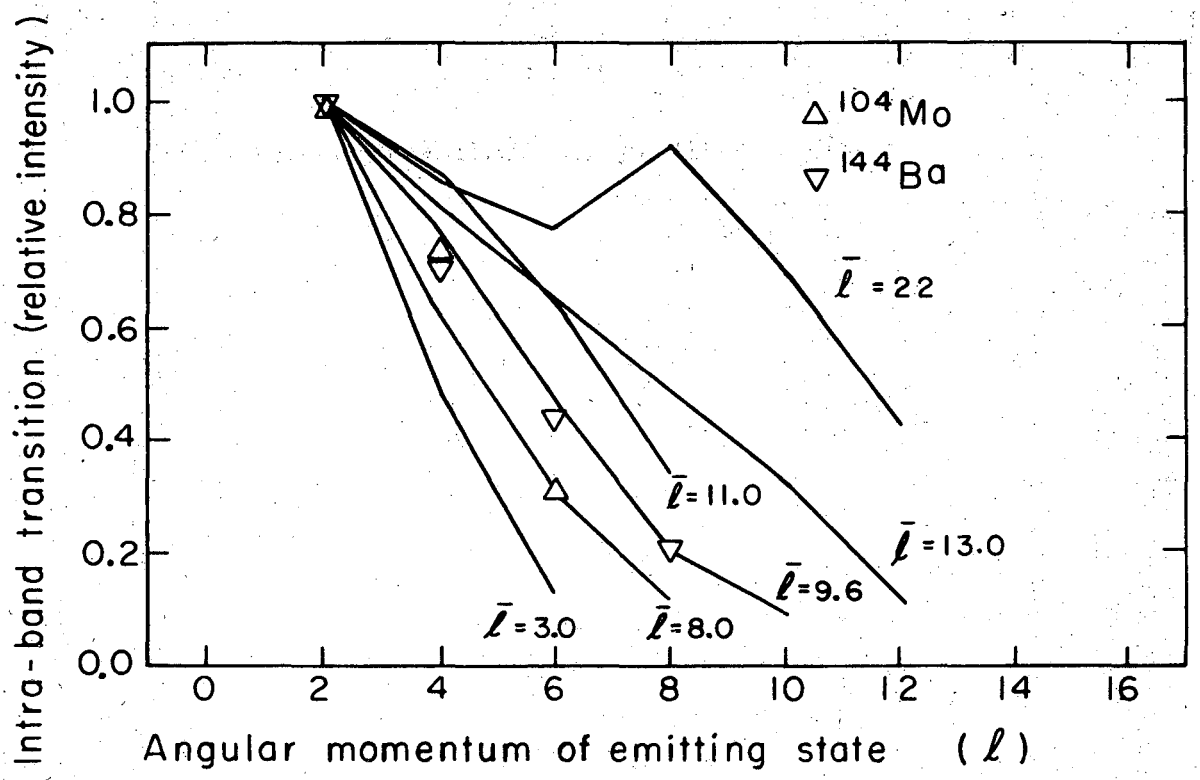

XBL706-3041

Fig. 6

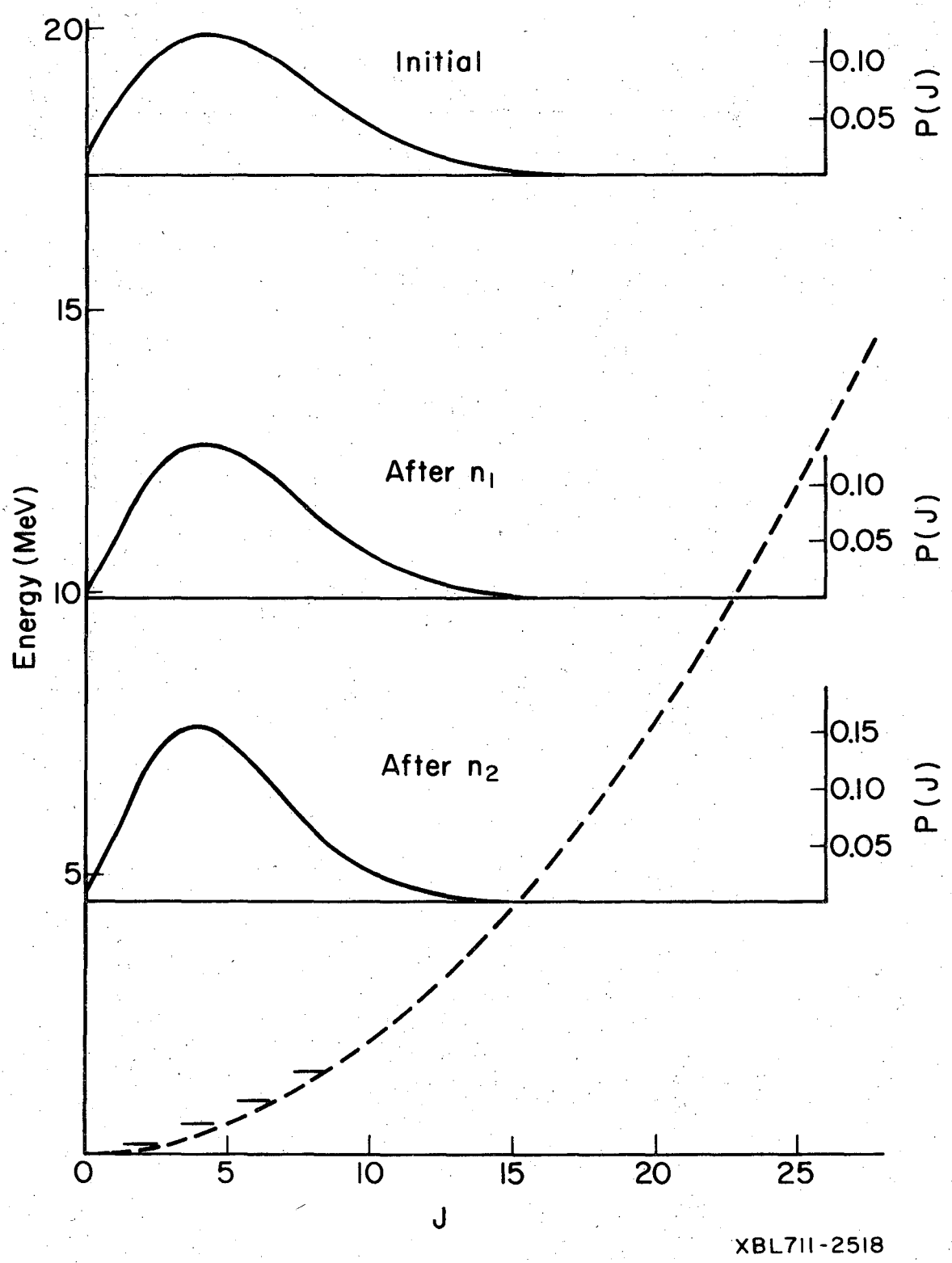
Initial
After n_1
After n_2
Energy (MeV)
20
15
10
5
0
5
10
15
20
25
J
0.10
0.05
P(J)
0.15
XBL711-2518

Fig. 7

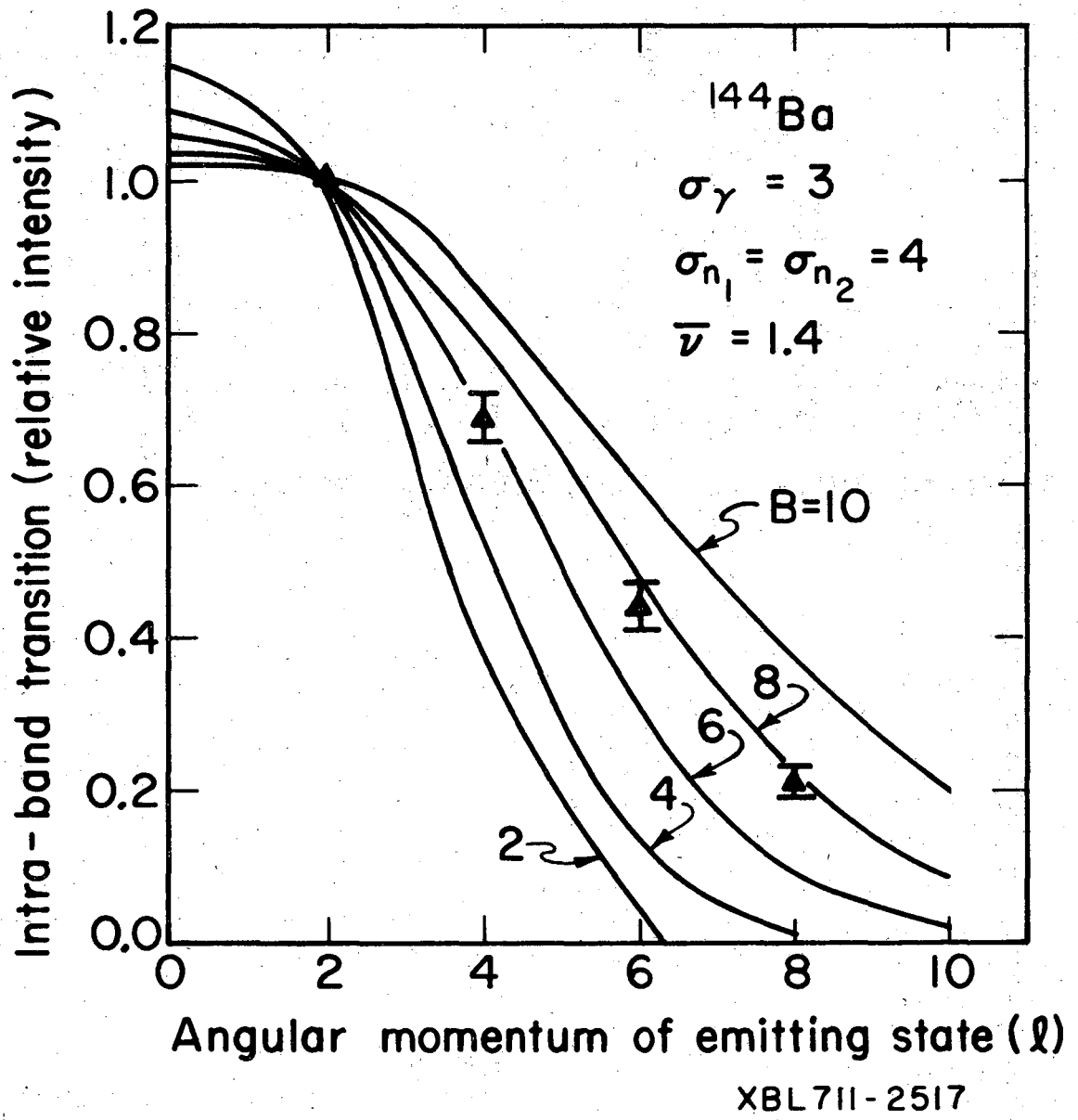
^{144}Ba
$\sigma_\gamma = 3$
$\sigma_{n_1} = \sigma_{n_2} = 4$
$\bar{\nu} = 1.4$
B=10
8
6
4
2
Intra-band transition (relative intensity)
Angular momentum of emitting state (ℓ)
0.0
0.2
0.4
0.6
0.8
1.0
1.2
0
2
4
6
8
10
XBL711-2517

Fig. 8

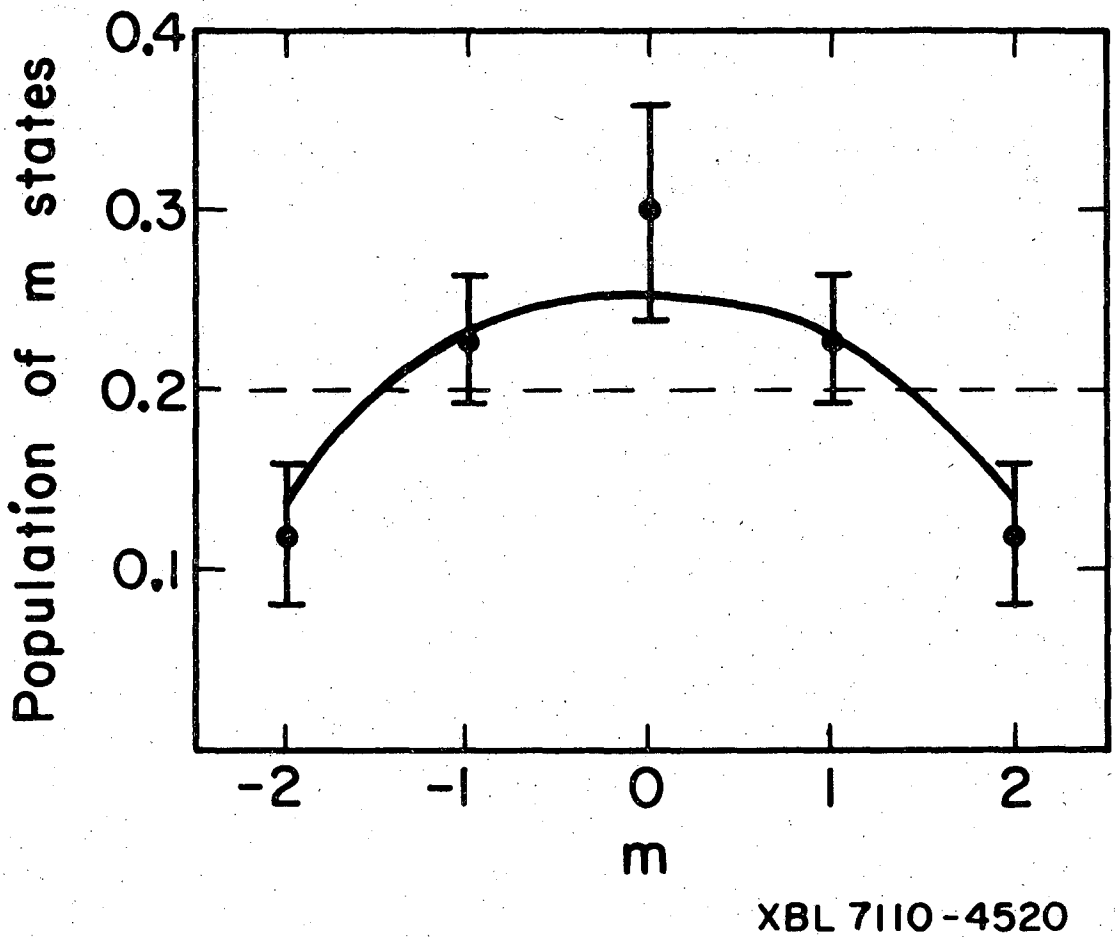

Fig. 9

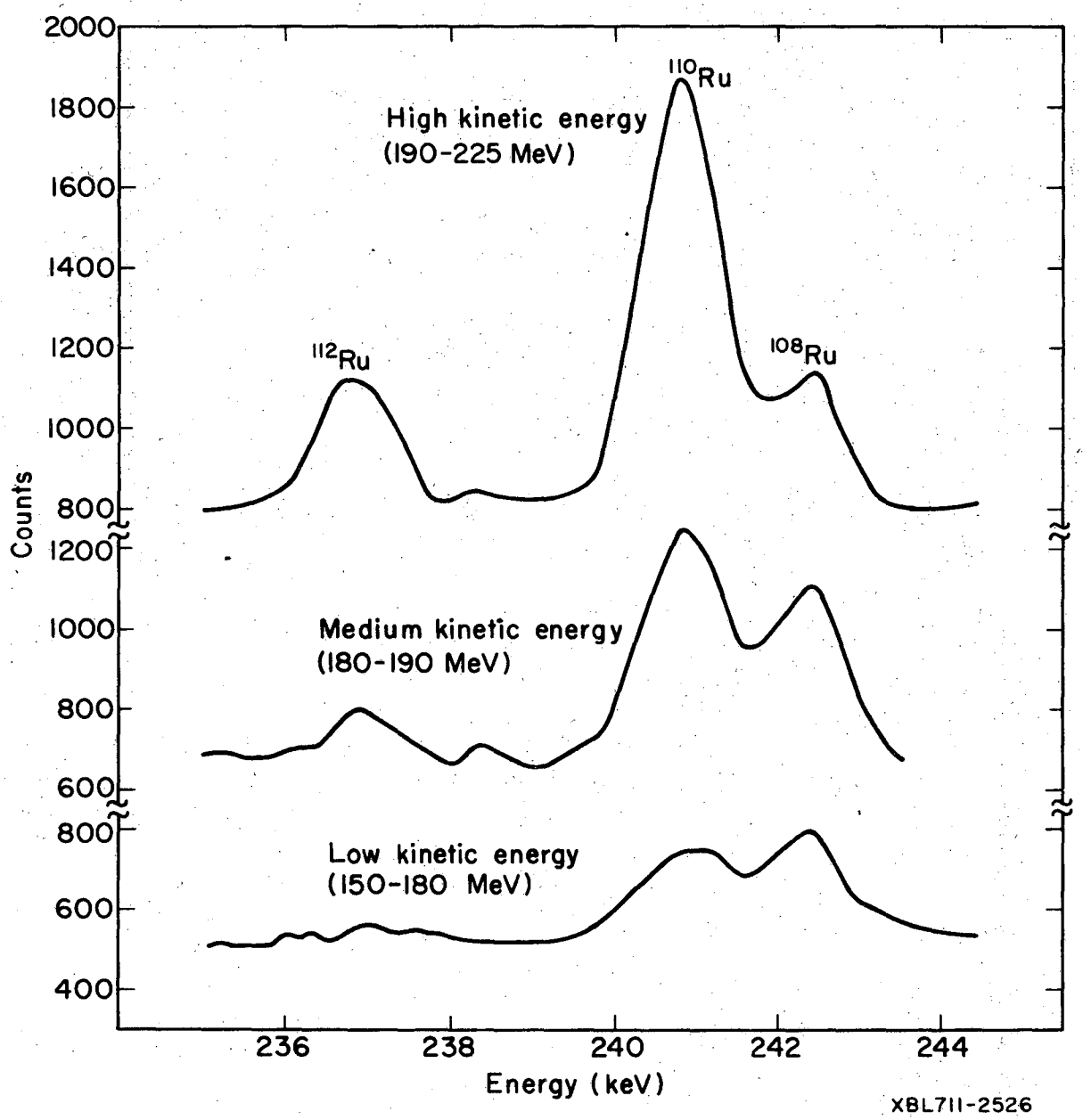
2000
1800
1600
1400
1200
1000
800
1200
1000
800
600
800
600
400
Counts
High kinetic energy
(190-225 MeV)
110Ru
112Ru
108Ru
Medium kinetic energy
(180-190 MeV)
Low kinetic energy
(150-180 MeV)
236
238
240
242
244
Energy (keV)
XBL711-2526

Fig. 10

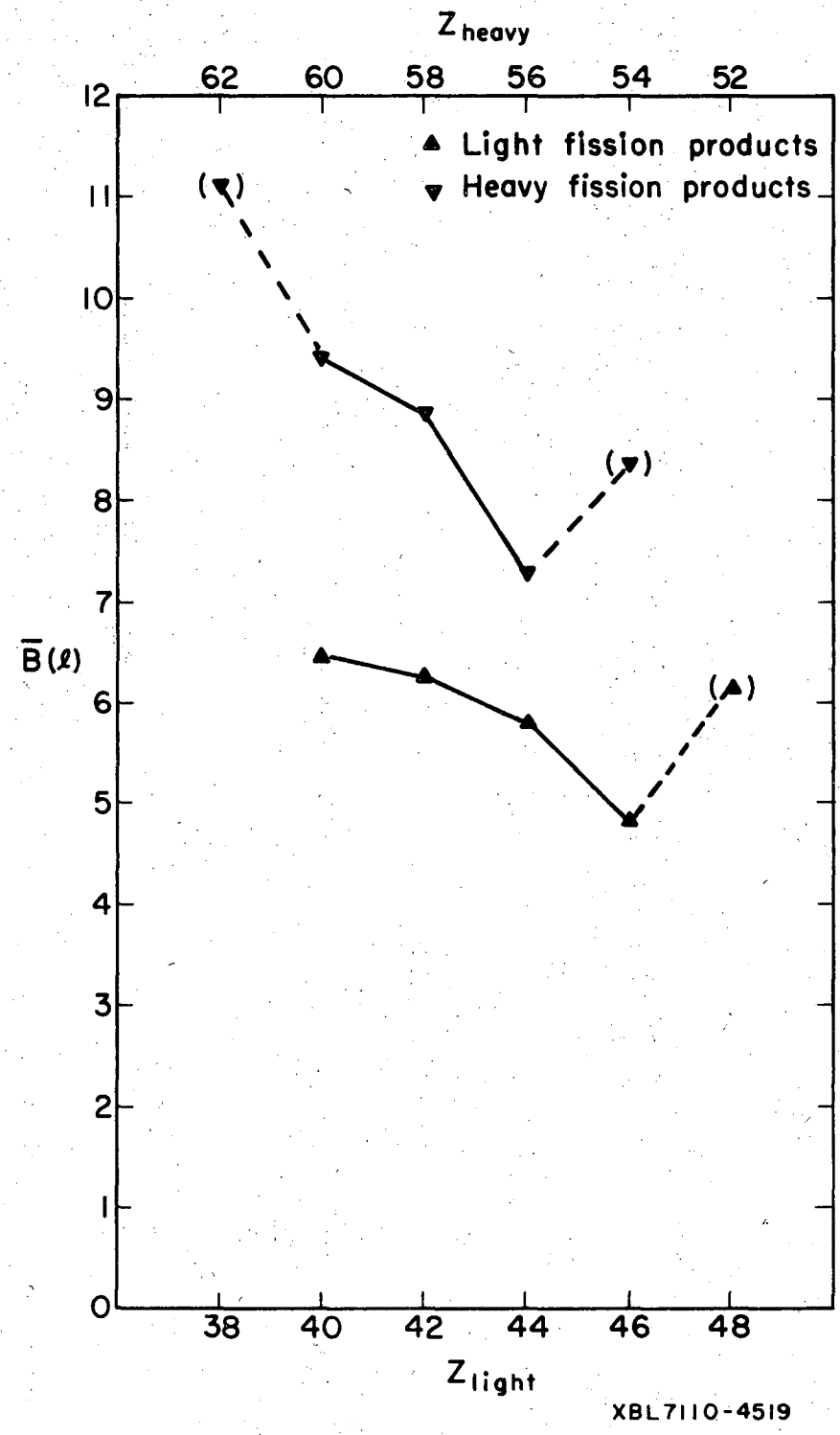
Z heavy
62
60
58
56
54
52
Light fission products
Heavy fission products
B̄(ℓ)
12
11
10
9
8
7
6
5
4
3
2
1
0
38
40
42
44
46
48
Z light
XBL7110-4519

Fig. 11

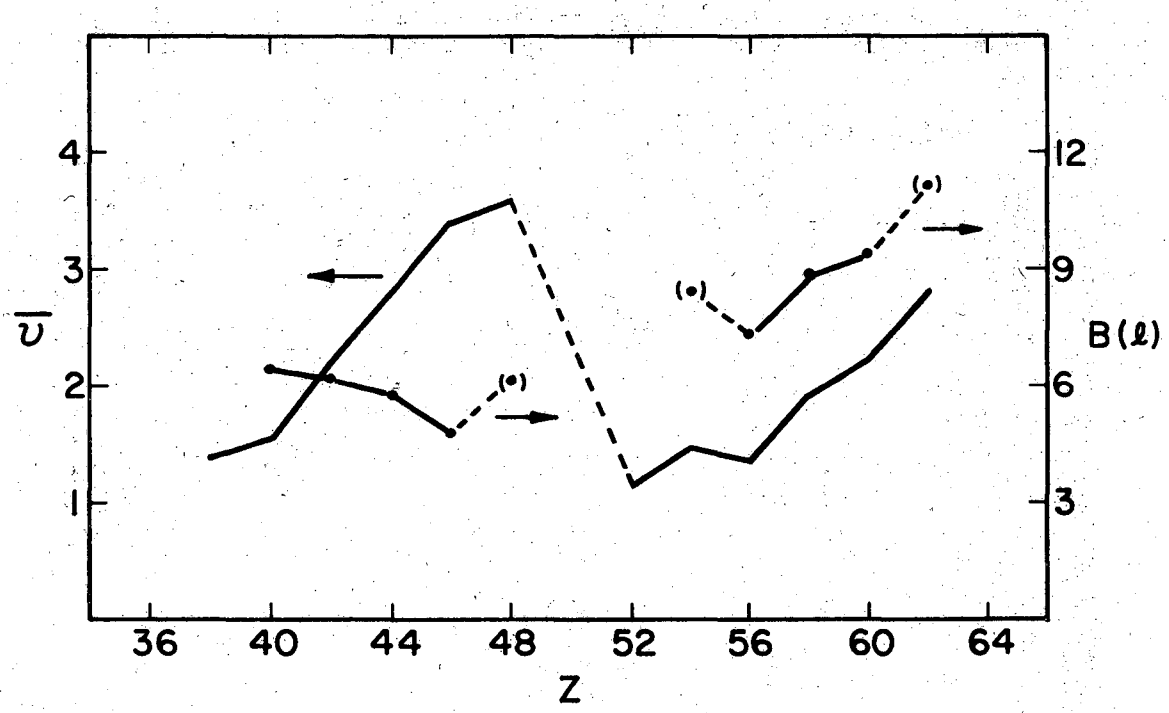

Fig. 12

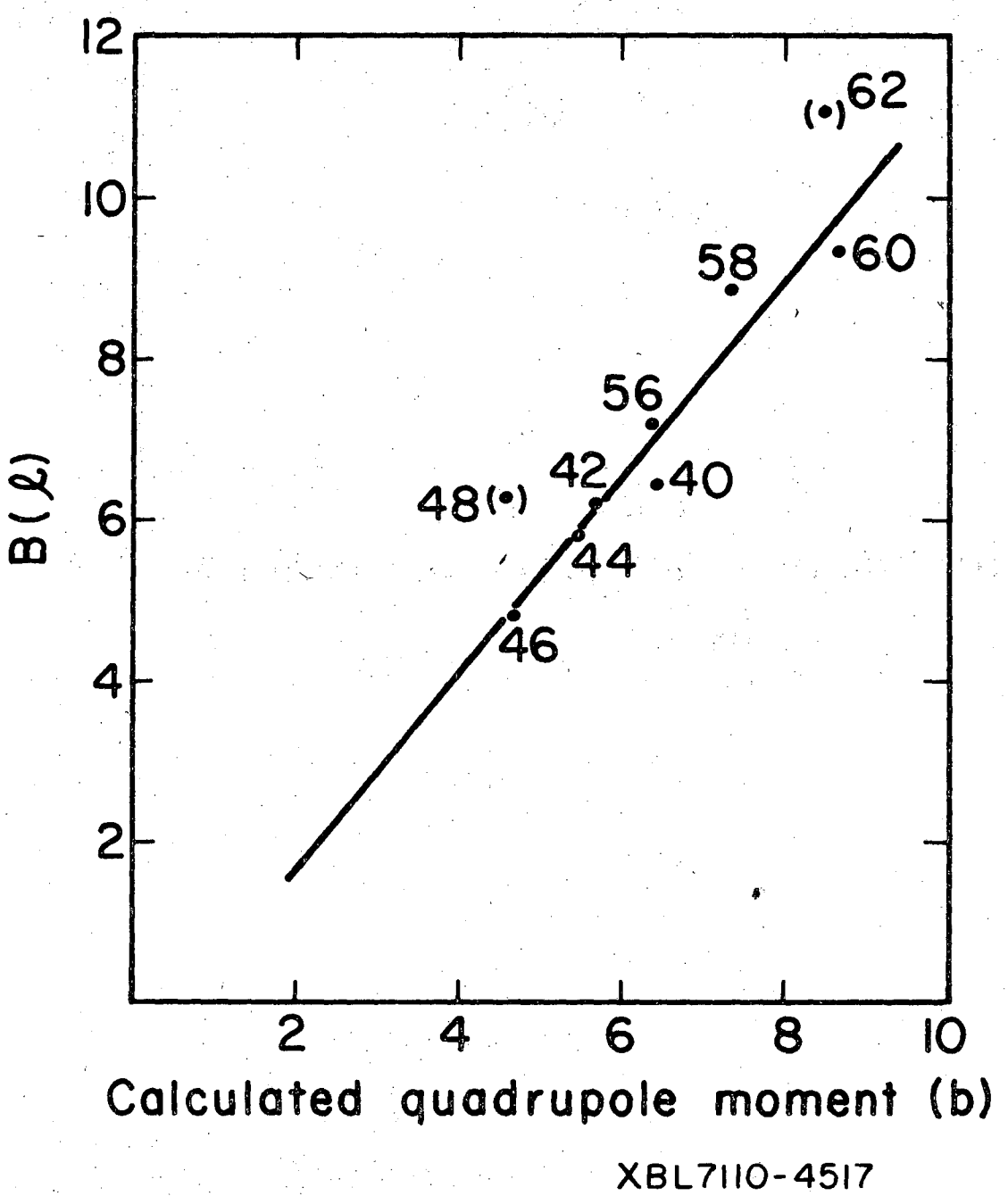
12
10
8
6
4
2
B(ℓ)
(•)62
58
•60
56
42
•40
48(•)
44
46
2
4
6
8
10
Calculated quadrupole moment (b)
XBL7110-4517

Fig. 13

LEGAL NOTICE

This report was prepared as an account of work sponsored by the United States Government. Neither the United States nor the United States Atomic Energy Commission, nor any of their employees, nor any of their contractors, subcontractors, or their employees, makes any warranty, express or implied, or assumes any legal liability or responsibility for the accuracy, completeness or usefulness of any information, apparatus, product or process disclosed, or represents that its use would not infringe privately owned rights.

TECHNICAL INFORMATION DIVISION
LAWRENCE BERKELEY LABORATORY
UNIVERSITY OF CALIFORNIA
BERKELEY, CALIFORNIA 94720